

ORIGINAL ARTICLE

Special Section: Tribute to Rien van Genuchten, Recipient of the 2023 Wolf Prize for Agriculture

Dimensionality and scales of preferential flow in soils of Shale Hills hillslope simulated using HYDRUS

Ying Zhao^{1,2}  | Jun Yi³ | Rongjiang Yao⁴ | Fei Li⁵ | Robert Lee Hill⁶ | Horst H. Gerke⁷

¹College of Resources and Environmental Engineering, Ludong University, Yantai, China

²Global Institute for Water Security, University of Saskatchewan, Saskatoon, Saskatchewan, Canada

³Hubei Province Key Laboratory for Geographical Process Analysis and Simulation, Central China Normal University, Wuhan, China

⁴State Key Laboratory of Soil and Sustainable Agriculture, Institute of Soil Science, Chinese Academy of Sciences, Nanjing, China

⁵Grassland Research Institute, Chinese Academy of Agricultural Sciences, Huhhot, China

⁶Department of Environmental Science and Technology, University of Maryland, College Park, Maryland, USA

⁷Leibniz Centre for Agricultural Landscape Research (ZALF), Research Area 1 "Landscape Functioning", Müncheberg, Germany

Correspondence

Ying Zhao, College of Resources and Environmental Engineering, Ludong University, Yantai, 264025, China.

Email: yzhaosoils@gmail.com

Rongjiang Yao, State Key Laboratory of Soil and Sustainable Agriculture, Institute of Soil Science, Chinese Academy of Sciences, Nanjing, 210008, China.

Email: rjyao@issas.ac.cn

Assigned to Associate Editor Majdi Abou Najm.

Funding information

National Natural Science Foundation of China, Grant/Award Number: 42320104006; Taishan Scholars Program, Grant/Award Numbers: 201812096, 202211185; National Institute of Food and Agriculture, Grant/Award Number: 1014496

Abstract

Preferential flow (PF) processes are governed by subsurface soil structures at various scales. Still, model validation and mechanistic understanding of PF are very lacking. We hypothesize that PF at hillslope and larger scales cannot be described and quantified when neglecting small-scaled spatially variable processes and simplifying the model dimensionality. The objective was to learn from comparing simulation results of multidimensional (1D, 2D, and 3D) and multiscale (pedon, catena, and catchment) modeling approaches with comprehensive datasets, and so as to evaluate PF simulations based on the Richards' equation (solved by the HYDRUS software). Results showed limited alignment between 1D simulations and soil moisture data, mainly affected by vertical changes in porosity, permeability, and precipitation features. 2D and 3D simulations outperformed 1D models. 3D simulations provided satisfactory description of PF dynamics at the pedon scale, considering accurate representations of soil and bedrock structures for three dimensions (vertical, horizontal, and surrounding area). In 2D simulations at the pedon scale, models incorporating dual-porosity and anisotropy of soils yielded more accurate predictions of water dynamics than single-porosity and isotropic models. Furthermore, the application of 2D simulation at the catena scale identify PF pathways owing to the enhanced representation of the hydraulic connectivity between different locations along the slope. The results confirmed the significance of multidimensional and multiscale modeling approaches

Abbreviations: BC, boundary condition; NSE, Nash–Sutcliffe efficiency; PF, preferential flow.

This is an open access article under the terms of the [Creative Commons Attribution](https://creativecommons.org/licenses/by/4.0/) License, which permits use, distribution and reproduction in any medium, provided the original work is properly cited.

© 2024 The Author(s). *Vadose Zone Journal* published by Wiley Periodicals LLC on behalf of Soil Science Society of America.

for PF simulations in hillslope hydrology. Considering the complexity and parameterization of 2D and 3D “bottom-up” physically based models in representing spatial variability within and between soil profiles and/or underlying bedrock geology, the results contribute to creating a modeling framework applicable to identify the PF processes and thus their implications in managing water resources.

1 | INTRODUCTION

The complexity of preferential flow (PF) is broadly acknowledged, and its quantification remains challenging (Vereecken et al., 2015). One problem is that PF may affect soil water flow, which depends on varying precipitation inputs, soil-terrain attributes, and moisture conditions. PF, as defined by Hendrickx and Flury (2001), includes all phenomena where water and solutes move along specific pathways, while bypassing a fraction of the porous matrix, causing irregular wetting patterns and varied rates of water movement within the soil layers (Freeze, 1972). Understanding PF dynamics is critical for explaining water flow through soils, designing monitoring schemes, and improving numerical models (Clark et al., 2015; Lin & Zhou, 2008). Early studies viewed PF primarily as one-dimensional rapid flow through macropores (e.g., Vogel & Roth, 2003), focusing on vertical flow in the unsaturated zone. However, recent studies emphasize its multidimensional nature (Fan et al., 2019), highlighting phenomena like fast flow through macropore, furrow flow from hydraulic property variability, and fingering flow from wetting front instability (Gao et al., 2018; Vereecken et al., 2015).

PF is common yet difficult to represent in hydrological models (Beven & Germann, 2013; Gu et al., 2018; Schulz et al., 2006) due to its scale-dependent nature related to subsurface structures and heterogeneities (Beven & Germann, 1982, 2013; Liu & Lin, 2015; Nimmo, 2012). Guo and Lin (2018) highlighted key challenges in developing PF models such as (1) difficulty in incorporating all influencing factors and their interactions controlling PF initiation and dynamics into physics-based models, (2) site-specific and condition-dependent influences of controlling factors on PF, and (3) challenges in representing hierarchical soil heterogeneity in models. PF varies from pore to catchment scale, with different characteristics at each scale (Hendrickx & Flury, 2001). Smaller ones influence larger scale processes (Bittelli et al., 2010), leading to a hierarchy of scales with increasing heterogeneity from soil profile to catchment (Blöschl & Grayson, 2001; Korres et al., 2015; McDonnell et al., 2007). A hierarchical categorization for watersheds may improve the identification of processes and boost forecasting capabilities (McDonnell et al., 2007).

The scale of model domains significantly affects PF predictions, with lateral resolution influencing soil water drainage

simulation. Many researchers believe the scales of existing catchment models are too vast to account for lateral soil water effects (Fan et al., 2019). Recently, the process of lateral PF along the bedrock surface has been incorporated into models (Dusek & Vogel, 2014), demonstrating that the simpler 1D model has a similar discharge prediction against a more complex 2D model. While many studies have explored uniform and equilibrium water flow in the vadose zone (e.g., Gerke et al., 2010; Scanlon et al., 2002), there is limited research on preferential and nonequilibrium flows (Jiang et al., 2023; Larsson & Jarvis, 1999; Yi et al., 2019). Few models address the combined impacts of heterogeneity, topography, and scale on hydrological fluxes (Bittelli et al., 2010; Clark et al., 2015; Ebel et al., 2007). Typically, modelers use plot-scale water flow descriptions for hillslope scale balance (Tromp-van Meerveld & Weiler, 2008), as the large-scale models have displayed limitations in the description of the small-scaled field heterogeneity. The 3D simulations of lateral flow, incorporating diverse soil properties and boundaries, have proven superior to 2D simulations (Fan et al., 2019; Loague et al., 2006; Mirus et al., 2007).

Another challenge is assessing various model uncertainties, such as soil and bedrock parameters and applied boundary conditions (BCs) (Loos et al., 2007). While research has primarily focused on single-porosity models for water flow, the mobile-immobile, dual-porosity, and dual-permeability models are needed for nonequilibrium flow (Beven & Germann, 1982; Durner, 1994; Gerke & van Genuchten, 1993a; Jarvis et al., 2016; Šimůnek et al., 2006). Current PF models, such as the dual-porosity and dual-permeability models, typically rely on distinguishing the hydraulic properties between the PF and surrounding soil matrix domains (Šimůnek et al., 2003). Complex landscape water movement models must account for lateral flow from factors like anisotropic hydraulic conductivity, topography, or geological setting (Buttle & McDonald, 2002; Maxwell & Kollet, 2008). Lateral flow at soil-bedrock interfaces is crucial for hillslope flow paths (Freer et al., 1997; Haga et al., 2005; Noguchi et al., 1999). Some models consider a permeable soil-bedrock interface, but fewer have been validated with data (Ebel et al., 2007; Todd et al., 2000). Based on virtual experiments, Hopp and McDonnell (2009) used a 3D model to study rain stormflow generation controls, but their model structure lacked PF representation. Models like HillVi (Weiler & McDonnell, 2007) focus on PF but struggle

with parameterizing the soil characteristics related to the PF occurrence at the hillslope scale.

Prior research at the Shale Hills watershed observatory using detailed soil moisture data revealed distinct landscape soil differences (Guo et al., 2014; Lin & Zhou, 2008) and common PF occurrences (Liu & Lin, 2015; Zhao et al., 2012). For instance, Liu and Lin (2015) found that clay content and topography contributed to 81% of the spatial variation in PF frequency. However, there is a knowledge gap on how spatial scale, soil heterogeneity, and bedrock permeability individually affect PF occurrences. First, we hypothesize that utilizing a physical-based model for soil water movement simulation, for example, via a widely used HYDRUS software (Kohne et al., 2004; Saito et al., 2006; Scanlon et al., 2002; Šimůnek et al., 2016; Twarakavi et al., 2008), can grasp the PF flow at the pedon scale, especially considering the differences of soil subsurface characteristics. The core question is whether small-scale HYDRUS code, with specific soil data, can replicate complex hydrological system behaviors like PF that usually occurred at a relatively larger spatial scale (Vereecken et al., 2015). Previous studies indicate that soil structure significantly influences water behaviors in models, but the effects of small-scale structures on PF were not well simulated (Fan et al., 2019). Challenges arise in representing physical processes, especially during intense rainfall. Furthermore, the complexity required in hydrological models remains debated (Tromp-van Meerveld & Weiler, 2008; Zhao et al., 2024). While a 3D model capturing nuanced water flow is ideal, it demands considerable computational power (Fan et al., 2019). Indeed, although model validation faces data constraints, it is unclear if accounting for more complexity improves accuracy. Thus, our second hypothesis is that a multidimensional modeling framework, associated with the level of model complexity, is helpful for identifying key processes governing PF. The multidimensional modeling approach, in which the effects of simplifications in lower dimension modeling are compared with results obtained with higher dimension models, can be useful in optimizing between the accuracy of process descriptions and computational efficiency of process-based model. However, to date, the literature lacks a comprehensive and detailed comparison between hillslope soil moisture data and PF predictions derived from a process-based model.

For this study, we simulated 1D vertical, 2D cross-sectional, and 3D hillslope domains from a well-known Shale Hills catchment dataset and analyzed and compared the results to identify the cross-scale importance of smaller scale effects. The objectives of this study are to (1) evaluate multidimensional modeling approaches for identifying key processes governing PF, (2) test dual-porosity and anisotropic models' ability to describe PF, and (3) analyze how soil-bedrock conditions affect PF occurrence. The results may offer a

Core Ideas

- The 3D model was better than 2D model to detect the preferential flow.
- A dual-porosity or anisotropy model produced more accurate predictions than a single-porosity or isotropy model.
- A model domain that considered fractured bedrock performed better than without it.

cross-scale modeling framework for PF simulation, which is essential for water resources or environmental applications.

2 | MATERIALS AND METHODS

2.1 | Experimental site and measurements

We used field monitoring data in the model simulations from collected between 2007 and 2010 in the 7.9-ha forested Shale Hills catchment in central Pennsylvania (Figure 1). Soil moisture monitoring indicated the presence of PF's existence and suggested that this water movement was influenced by soil properties such as soil type, soil depth, permeability, and location (Zhao et al., 2012).

The Shale Hills catchment has a humid continental climate, with mean monthly temperatures ranging from -3°C in January to 22°C in July and yearly rainfall of 980 mm (National Weather Service, State College, PA). This V-shaped catchment has slopes up to 25%–48%, elevations between 256 and 310 m, and is crossed by a first-order stream. It is built on a 300-m deep fractured Rose Hill Shale and features a maple-oak-hickory forest. The soils, mainly silt loam and silty clay loam, were derived from shale colluvium and have numerous shale fragments (Table 1).

Sensors were installed at four sites to monitor soil conditions in different terrains as follows (Figure 1 and Table 1): Weikert series on a hilltop, Rushtown series upslope, Rushtown series midslope, and Ernest series valley floor near a stream (Sites 74, 53, 51, and 15, respectively). Each site had sensors to measure soil water content, soil matric potential, and soil temperature. The study mainly focused on 10-min interval soil moisture data using capacitance-type soil moisture probes (ECH₂O-5 or ECH₂O-10), with $\pm 3\%$ accuracy and 0.1% resolution (Decagon Devices Inc.). We evaluate PF occurrence using a soil moisture response time method. That is, the occurrence of PF was observed when a lower soil horizon responded to rainfall earlier than the one above (Lin & Zhou, 2008), as indicated in Figure 2 for sites 74 and 51.

TABLE 1 Soil and landscape features displayed for the monitoring sites 74, 54, 51, and 15 in the Shale Hills catchment of Pennsylvania.

Soil series	Site number	Landform position	Slope (%)	Soil horizon	Sensor depth (cm)	Depth to bedrock (cm)	Rock fragment mass ratio (%)	Soil texture				
Weikert	74	Nearly planar slope	23.8	Oe-A	5	22	0	Silt loam				
				A	8			Silt loam				
				A-CR	10		60	Silt loam				
				CR	17		90	Silt loam				
				R	37							
Rushtown	53	Swale, upslope	38.4	A	10	>150	5	Silt loam				
				Bw1	22		5	Silt loam				
				Bw2	44		5	Silt loam				
				Bw3	73		5	Silty clay loam				
				C	123		80					
				Oe	5	>300						
				A-Bw1	8		5	Silt loam				
Rushtown	51	Swale, midslope	13.1	Bw1	12		5	Silt loam				
				Bw1	15		5	Silt loam				
				Bw2	22		5	Silt loam				
				Bw3	40		5	Silty clay loam				
				BC	68		50	Silty clay loam				
				BC-C1	92		50	Silty clay loam				
				C1	122		80					
				C2	162		80					
				Ernest	15	Valley floor	6.6	A	13	>300	0	Silt loam
								AE-Bw	20		0	Silt loam
Bt	41		0					Silty clay				
Bt-C1	52		0					Silty clay				
C2	72		80 (soft)					Sandy loam				
C2-C3	85		0					Clay				
C4	109		90 (soft)	Sandy loam								

Note: Sensor depth refers to the burial depth of a sensor used for measuring soil moisture. Rock fragments are all shale channers of 2- to 150-mm thick, many are soft or very soft. Soil horizons in bold are those that were selected to simulate preferential flow. Modified from Lin and Zhou (2008) and Liu and Lin (2015).

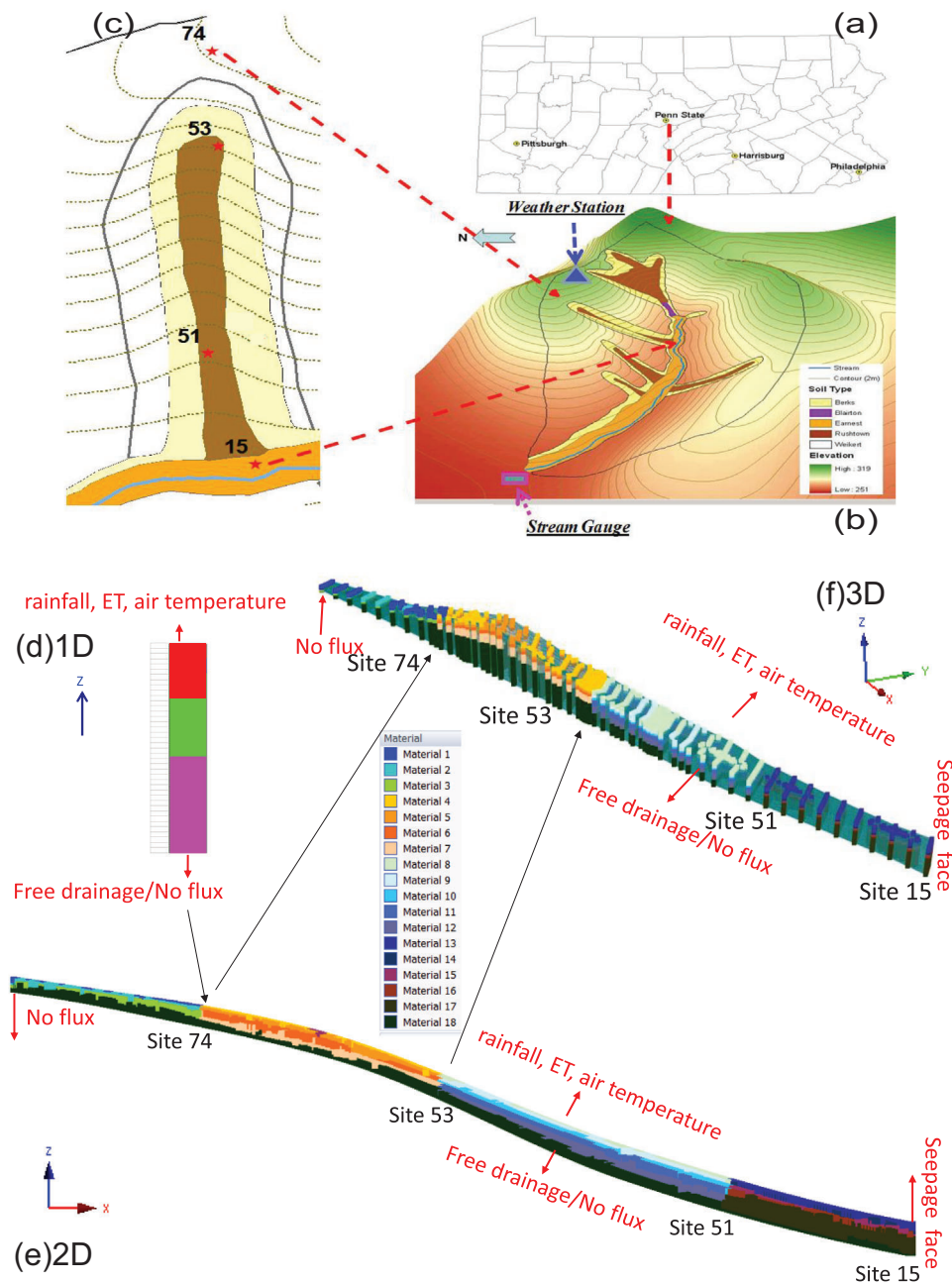


FIGURE 1 Location (a), shape (b), and the study hillslope (c) of the Shale Hills catchment, and graphical representation of the HYDRUS-1D (d), -2D (e), and -3D (f) simulation model domains with different soil materials (presented by different colors) for the monitoring sites 74, 53, 51, and 15 and the applied boundary conditions. ET, evapotranspiration.

Note that the term “PF” encompasses various flow types like macropore, unstable, and funnel flow. While we do not have set criteria for determining the type of PF (Guo & Lin, 2018; Hendrickx & Flury, 2001; Nimmo, 2012), our method using soil moisture sensor networks (i.e., nonsequential soil moisture response method) might underestimate its presence as it does not account for all possible phenomena.

To determine soil hydraulic properties (Table 2), representative soil horizons were sampled from each soil pit. The saturated hydraulic conductivities (K_s) were determined with

the falling head method (Zhao et al., 2010) using large (30-cm diameter and 20-cm long) and intact soil cylinder sampled in both vertical and horizontal directions (Lin et al., 2006). The differences between the lateral and vertical values indicated anisotropy of K_s , for example, the horizontal K_s values were almost 10 times higher than the vertical values for the B horizon and in the vicinity of the bedrock fractures (Table 2). This difference is ascribed to a platy structure leading to a higher pore continuity in the horizontal direction along the aggregate surfaces and fractures. This higher continuity has

TABLE 2 Hydraulic parameters for the different monitoring sites: (a) single-porosity model with van Genuchten–Mualem parameters obtained from inverse modeling with field data, (b) dual-porosity model parameters obtained from inverse modeling with field data (immobile water parameters indicated by subscript im, and mobile water parameters indicated by subscript mo).

Site	Soil depth (cm)	(a) Single-porosity model				(b) Dual-porosity model			
		θ_r ($\text{cm}^3 \text{cm}^{-3}$)	θ_s ($\text{cm}^3 \text{cm}^{-3}$)	α (cm^{-1})	n (-)	$K_s (K_v/K_h)$ (cm day^{-1})	$\theta_{s_{\text{mo}}}$ ($\text{cm}^3 \text{cm}^{-3}$)	$\theta_{s_{\text{im}}}$ ($\text{cm}^3 \text{cm}^{-3}$)	a_w ($\text{cm}^{-1} \text{day}^{-1}$)
74	0–5	0.02	0.26	0.247	1.523	316/80	0.16	0.1	1.84E-04
	5–15	0	0.29	0.036	1.714	3003/265	0.19	0.1	1.10E-03
	15–30	0.03	0.25	0.02	1.547	301/320	0.1	0.15	7.20E-01
	30–76	0.04	0.4	0.022	1.473	109/560	0.15	0.25	1.93E-04
53	0–10	0	0.44	0.007	2.277	1123/159	0.35	0.09	5.95E-04
	10–40	0.04	0.38	0.008	2.089	5/245	0.3	0.08	2.07E-05
	40–80	0.04	0.33	0.021	1.594	293/370	0.18	0.15	5.58E-03
	80–149	0.01	0.26	0.006	1.846	318/690	0.15	0.11	5.93E-04
51	0–10	0.03	0.4	0.08	1.58	150/116	0.36	0.04	2.00E-04
	10–30	0.05	0.45	0.011	3.461	602/270	0.35	0.15	9.30E-03
	30–50	0.03	0.33	0.012	2.278	144/2100	0.2	0.16	2.62E-03
	50–100	0.05	0.3	0.037	1.801	299/410	0.15	0.12	2.06E-03
15	100–236	0.03	0.3	0.009	2.095	2/450	0.16	0.14	6.65E-03
	0–20	0.05	0.45	0.023	2.228	27/170	0.39	0.06	5.39E-04
	20–52	0.08	0.43	0.013	1.962	2485/230	0.33	0.1	1.13E-05
	52–83	0.12	0.42	0.012	1.716	273/320	0.29	0.15	2.02E-04
83–91	83–91	0.1	0.37	0.1	1.45	100/310	0.25	0.12	2.00E-04
	91–260	0.13	0.35	0.014	1.355	57/130	0.2	0.18	2.04E-04

Note: θ_r and θ_s are the residual and saturated soil water contents, respectively; α and n are empirical shape parameters in the van Genuchten–Mualem model; K_s is the saturated hydraulic conductivity, K_v and K_h are the vertical and horizontal saturated hydraulic conductivities, respectively; and a_w is a first-order mass transfer coefficient.

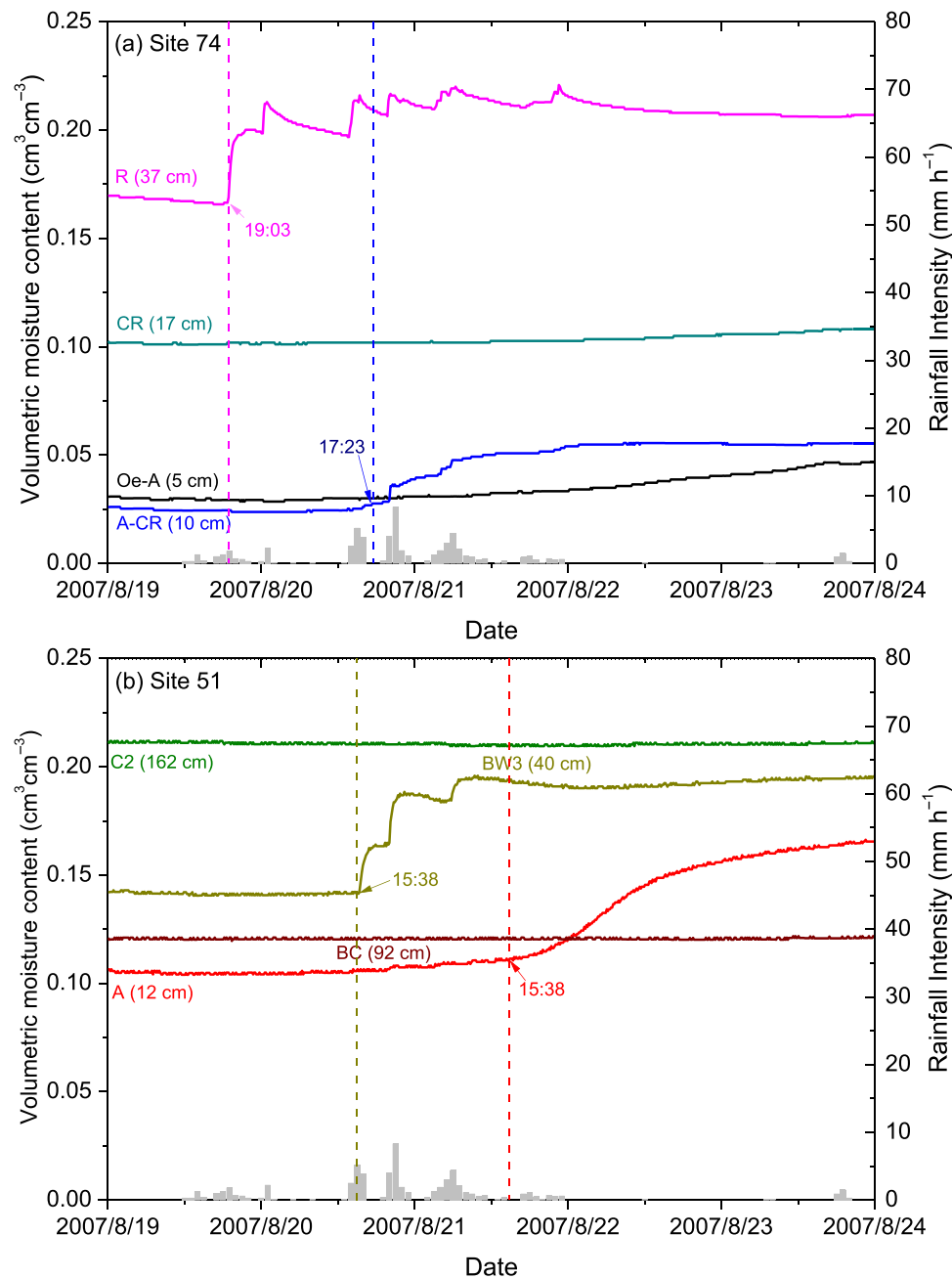


FIGURE 2 Volumetric soil moisture content and rainfall intensities during the drier period of August 19–24, 2007 at sites 74 (a) and 51 (b). The time at which soil moisture contents started to increase is indicated by bold arrows. The different colored lines identify the soil horizons with the horizon layer in capital letters and the depth of soil moisture sensor in parenthesis. The dash line indicates the occurrence of preferential flow.

helped with how a hydrologic and geochemical model should be developed (Fan et al., 2019). The water retention characteristics were determined with the pressure plate method (Zhao et al., 2010), and the parameters of the soil hydraulic functions were fitted using the RETC (REtention Curve) code (van Genuchten et al., 1991). The soil texture, bulk density, and total carbon content were determined using disturbed soil samples (Zhao et al., 2010). The precipitation and weather data required to estimate potential evapotranspiration were recorded by an in situ automatic micrometeorological station (Lin et al., 2006). Root density, leaf area index, and coverage

of trees were based on the local measurements (Brantley et al., 2018), and a groundwater level sensor (Odyssey Capacitance Water Level Logger, Dataflow Systems Ltd) was installed at site 15 (Figure 1); more details can be found in Brantley et al. (2018).

2.2 | Soil water flow modeling

We used HYDRUS software package (1D, 2D, and 3D) (Šimůnek et al., 2016) for the simulations, comparing

the baseline HYDRUS-2D with HYDRUS-1D and 3D regarding model dimension issues (Table 3). Using the calibrated HYDRUS-2D, we examined uncertainties like soil properties, bedrock features, and applied BCs to study PF.

The HYDRUS codes solve Richards' equation for uniform water flow in variably saturated domains. The modified form of Richards' equation for HYDRUS-1D was well described in Zhao et al. (2023). The governing flow equation for HYDRUS-2/3D is given as follows:

$$\frac{\partial \theta}{\partial t} = \frac{\partial}{\partial x_i} \left(K(K_{ij}^A \frac{\partial h}{\partial x_j} + K_{iz}^A) \right) - S \quad (1)$$

where θ is the volumetric water content ($L^3 L^{-3}$), h is the pressure head (L), S is a sink term (T^{-1}), x_i ($i = 1, 2, 3$) are the spatial dimensions (L), t is the time (T), and K_{ij}^A and K_{iz}^A are the components of a dimensionless anisotropy tensor K^A , and K is the unsaturated hydraulic conductivity ($L T^{-1}$), respectively. We used the van Genuchten–Mualem model (van Genuchten, 1980) for describing the hydraulic functions as follows:

$$S_e = \frac{\theta - \theta_r}{\theta_s - \theta_r} = \frac{1}{(1 + |\alpha h|^n)^m} \quad (2a)$$

$$K = K_s S_e^l [1 - (1 - S_e^{1/m})^m]^2 \quad (2b)$$

where S_e is the effective saturation, θ_s and θ_r are the saturated and residual water contents ($L^3 L^{-3}$), respectively, the symbols α (L^{-1}), n , and m are the shape parameters, with $m = 1 - 1/n$, K_s is the saturated hydraulic conductivity ($L T^{-1}$), and l is a pore connectivity parameter, which was set to 0.5.

A nonequilibrium dual-porosity model of the mobile–immobile type was also used in addition to the single-porosity model (Equation 1). This dual-porosity model assumes that the pore system is partitioned into an inter-aggregate or fracture pore domain and an intra-aggregate pore domain without macroscopic water flow (Šimůnek et al., 2003). This conceptualization leads to a two-region mobile–immobile type flow model that partitions the liquid phase into a mobile, θ_{mo} , and an immobile (or stagnant), θ_{im} , water content ($L^3 L^{-3}$), with $\theta = \theta_{mo} + \theta_{im}$. Thus, the models incorporate the effects of PF using the dual-continuum concept. The coupled dual-porosity water flow model was described as follows (Gardenas et al., 2006):

$$\frac{\partial \theta_{mo}}{\partial t} = \frac{\partial}{\partial x_i} \left(K_{ij} \frac{\partial h_{mo}}{\partial x_j} + K_{iz} \right) - S_{mo} - \Gamma_w \quad (3a)$$

$$\frac{\partial \theta_{im}}{\partial t} = -S_{im} + \Gamma_w \quad (3b)$$

where S_{mo} and S_{im} are the sink terms for the mobile and immobile regions, respectively (T^{-1}) and Γ_w is a first-order water

TABLE 3 Design of the multidimensional, that is, 1D, 2D, and 3D modeling approaches and corresponding comparisons used in the study.

Simulation	Model dimension	Soil water model	K_s	Bottom boundary	Simulation period	Scale
0	Model calibration	VG and DP	Iso	IB (no flux)	Hourly: 2007.07.01–2007.08.31	Pedon
comparison of model dimension						
1	2D (baseline)	VG	Iso	IB (no flux)	Hourly: August 19, 2007–August 24, 2007 Daily: January 1, 2007–December 31, 2007 Yearly: January 1, 2008–December 31, 2010	Pedon, catena
2	1D	VG	Iso	IB (no flux)	Hourly: August 19, 2007–August 24, 2007 Daily: January 1, 2007–December 31, 2007	Pedon
3	3D	VG	Iso	IB (no flux)	Hourly: August 19, 2007–August 24, 2007 Daily: January 1, 2007–December 31, 2007	Pedon, catena, catchment
comparison of model uncertainty with the baseline						
4	2D	DP	Iso	IB (no flux)	Daily: January 1, 2007–December 31, 2007	Pedon, catena
5	2D	VG	Ani	IB (no flux)	Daily: January 1, 2007–December 31, 2007	Pedon, catena
6	2D	VG	Iso	FB (free drainage)	Daily: January 1, 2007–December 31, 2007	Pedon, catena

Abbreviations: Ani, anisotropy K_s ; DP, dual-porosity model; FB, fractured bedrock; IB, impermeable bedrock; Iso, isotropy K_s ; VG, single-porosity model.

transfer term for describing the exchange between the inter- and intra-aggregate pore domains (T^{-1}), here based on the difference in the pressure head between the mobile (subscript mo) and the immobile (subscript im) domains (Gerke & van Genuchten, 1993b) as:

$$\Gamma_w = \alpha_w (h_{mo} - h_{im}) \quad (3c)$$

where α_w is a first-order mass transfer coefficient ($L^{-1} T^{-1}$):

$$\alpha_w = \frac{\beta}{d^2} K_a(h) \gamma_w \quad (3d)$$

where d is an effective diffusion path length (i.e., half the aggregate width) (L), β is a shape factor that depends on the geometry of the soil aggregates (-), γ_w is a scaling factor (-), and K_a is the effective hydraulic conductivity of the fracture–matrix interface ($L T^{-1}$) determined as a simple arithmetic average involving both h_{mo} and h_{im} as follows:

$$K_a(h) = 0.5[K_a(h_f) - K_a(h_m)] \quad (3e)$$

2.3 | Model domain, initial, and BCs

The V-shaped study area in the Shale Hills catchment is used in our model test due to the sub-catchment being typical and well-monitored. This area represented in a 3D simulated domain (see Figure 1d), measures 85 m in length, 3–8 m in width, and 1–4 m in depth with a slope ranging from 7% to 38% (Figure 1 and Table 1). Based on soil horizon data, soil profiles are divided into 18 materials with depth-specific hydraulic properties: four layers (materials in Figure 1) for both hilltop (site 74) and upslope (site 53) and five layers for both midslope (site 51) and the valley floor (site 15) (Table 2). To compare with the 3D domain, the 2D simulation represented the transect along the slope from sites 74 to 51 (see Figure 1e), while the 1D simulation represented a vertical soil profile consisting of these heterogeneous layers located at the different monitoring sites (Figure 1f and Table 1). The 3D domain uses the Shale Hills hillslope digital elevation model (DEM) derived from 2006 LiDAR data (Lin et al., 2006). About 40,000 LiDAR points were converted into a 1 m \times 1 m DEM using ArcGIS 9.2 (ESRI Inc.). These data generated a finite element mesh of 46,200 nodes and 80,959 3D triangular prism elements, with a denser grid in the topsoil and around layer boundaries for ensuring numerical stability.

Initial conditions were established using linear interpolation of soil moisture at varying depths. Potential evapotranspiration was calculated using the Hargreaves equation (Hargreaves & Samani, 1985) and adjusted for water interception for the upper BC (Zhao et al., 2010). The side boundaries

of the model domain were set with specific conditions such as no flux at the upslope and edges, seepage face at the lower part (Figure 1). At the bottom, BCs were set differently depending on the considered modeling approach, as defined in Table 3. The minimum pressure head was -1500 kPa at the top, and root water uptake was based on the Feddes model (Feddes et al., 1978), with a maximum rooting depth of 100 cm, and most roots in the upper 50 cm of soil.

2.4 | Model calibration and implementation

We calibrated the HYDRUS-2D model using 2 months of data from July to August 2007 and used the measured soil hydraulic parameters as initial values and the measured soil water contents as variables in the objective function (Figure S1). Soil texture, varying from loamy sand to sandy loam, affected porosity and pore size distribution (Table 1) as reflected in depth-related hydraulic parameters (Table 2). For example, Weikert soil had lower water content and shallow R horizon, while the Rushtown soil had a deeper profile with more water. We optimized the hydraulic parameters using the inverse method, adjusting the van Genuchten–Mualem parameters α , n , and K_s (Table 2), while keeping the measured values of θ_s and θ_r unchanged. In the dual-porosity model, only α_w and θ_s were calibrated and θ_r , n , and K_s were kept the same as for the single-porosity model (Table 2). The θ_r value was assumed to equal zero for the mobile region as suggested by Clothier et al. (1995), who assumed that residual water is only present in the immobile region. The calibrated soil hydraulic parameters provided better simulations results than the uncalibrated (e.g., measured) ones (Figure S1) and were used in all subsequent HYDRUS simulations.

The 2D model calibration was chosen as it encompasses the main flow paths (vertical and lateral along the hillslope) and dominant hydrological processes, with less parameter estimation uncertainty and reduced risk of over-fitting as compared to the 3D model. The spatial variation and temporal dynamics of PF in soils can be jointly controlled by a complex interaction among landforms, soil properties, initial soil wetness, and rainfall characteristics (Guo & Lin, 2018). For consistent model dimension comparisons, we also need to utilize consistent values of the hydraulic parameters (Table 2). The single-porosity model was applied to simulate flow in 1D-vertical profiles, 2D hillslopes, and in 3D to account for domains with spatially distributed properties. The 1D single- versus dual-porosity simulations (e.g., simulation 4 in Table 3) were used to evaluate effects of nonequilibrium flow due to soil aggregation and a macropore network at pedon scale. The 2D hillslope simulations allowed evaluating effects of lateral flows due to spatially variable properties along the slopes, such as funnel flow induced by impeding layers. The

3D simulation allowed addressing additional flow processes such as lateral convergence at catchment scale. The simulations scenarios were spanning three scales: pedon (point), catena (hillslope), and V-shaped catchment as follows: the pedon scale was characterized by the 1D, 2D, and 3D models, the catena or hillslope scale by both 2D and 3D models, and the catchment scale solely by the 3D model (Table 3).

The simulations 4–6 (Table 3) aimed at testing the calibration (simulation 0) using field data from outside of the calibrated period as suggested earlier (Melsen et al., 2016). For the analysis of model flexibility, we used three temporal scales in our simulations depending on data availability (Table 3): minute-based values for quick water redistribution after rainfall and PF assessment (during August 19–24, 2007), daily values for water dynamics within a hydrological year (during 2007), and annual values for long-term water cycle predictions (during 2007–2011).

2.5 | Model uncertainty and performance assessment

Model uncertainties were expected due to soil hydraulic parameterization and effects of assumed BCs (Zhao et al., 2023). The impact of anisotropic hydraulic properties on PF was explored by comparing simulation results obtained with anisotropic and isotropic K_s values. The effect of fractured shale bedrock was tested using either permeable (free drainage) or impermeable (no flux) lower BCs (Table 3).

In addition to the graphical comparison of simulated and measured results, root mean square error, RMSE, and the Nash–Sutcliffe efficiency, NSE, were used to evaluate the model performance (e.g., Bittelli et al., 2010; Ebel et al., 2007):

$$\text{RMSE} = \sqrt{\frac{1}{N} \sum_{i=1}^N (P_i - O_i)^2} \quad (4a)$$

$$\text{NSE} = 1 - \frac{\sum_{i=1}^N (P_i - O_i)^2}{\sum_{i=1}^N (O_i - \bar{O})^2} \quad (4b)$$

where N is the number of observations, P_i and O_i are the simulated (predicted) and measured (observed) values, respectively, and \bar{O} is the mean of the observed values. The RMSE is inversely proportional to model efficiency, with smaller RMSE values indicating better model performance. The NSE statistic ranges between $-\infty$ and 1, with 1 indicating a perfect match between observed and modeled values.

3 | RESULTS

3.1 | Performance of multiple dimensions modeling approaches

The single-porosity Richards-based models simulated the soil moisture dynamics in various soil depths induced by rainfall infiltration as exemplified by 1D, 2D, and 3D model predictions versus measured soil moisture time series' for sites 74 and 53 (Figure 3). The 3D model of the V-shaped catchment provided the best predictions of soil moisture for these monitoring sites in terms of the lowest RMSE values (Table 4). The PF phenomenon seemed to be better described by 2D or 3D modeling approaches than with the 1D simulation. For example, during the period of August 19–24, 2007, for the pedon-scale comparisons, only 3D modeling simulated the timing of the PF occurrences accurately. The 3D model simulated an earlier soil moisture increases in the R horizon (37-cm depth) than in the soil layer above; the 1D and 2D approaches simulated the larger rain-induced frequent increase in soil moisture at site 74 (Figure 3a). Similarly, at site 51, the 3D simulation results matched with the measured soil moisture values at the deeper 40-cm soil depth by reproducing earlier and large increases compared to measured moisture values at the shallower 12-cm soil depth; however, the 1D simulation did not reflect this moisture difference attributed to PF (Figure 3b). The accuracy of 2D modeling in PF simulation is between the 3D and 1D (Table 4). The RMSE values are all smaller than 0.1, with the smallest errors for the 3D simulations and the largest errors for the 1D simulations. Similarly, the NSE values range from -3.8 to 0.74 , with the largest values for the 3D simulation. The negative NSE values are attributed to a few poorly simulated soil water content values that lag behind the measured ones (e.g., see Figure 3).

For the 1-year hydrological simulations at pedon scale (Figure 4), the 1D model (simulation 2) underestimated the soil moisture because it did not consider the lateral flow contributions. In contrast, the 2D model (simulation 1) considered the slope-topographic effects and performed better, but the predicted results were not as good as those obtained with the 3D model (simulation 3). In the topsoil layer at site 74, the 3D simulation outperformed the 2D simulation, even though the 2D simulation was sensitive in capturing rainwater input (Figure 4). For the 4-year period, the 2D model described the soil hydrological processes similarly and accurately as for the 1-year simulation (Figure S2). The annual water balance simulated with the 2D model in 2007 (Figure S3), indicating that 38% of the precipitation drained (i.e., 6% seepage flux as streamflow and 32% groundwater recharge), 35% was evaporation, 19% was transpiration, and 8% went into soil water

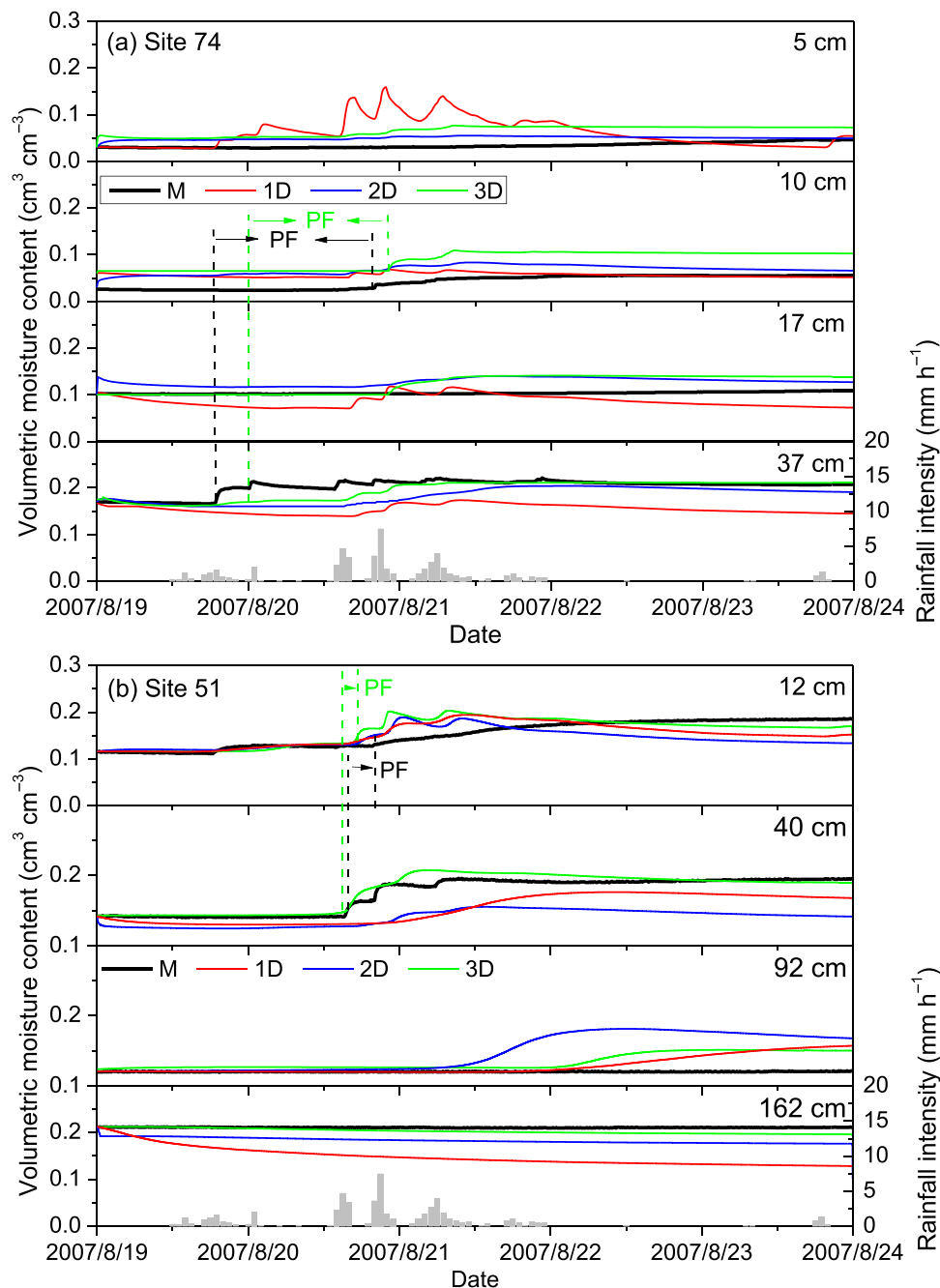


FIGURE 3 Time series of measured (M) and simulated soil moisture and rainfall intensities during the period of August 19–24, 2007 at sites 74 (a) and 51 (b) for the HYDRUS-1D, -2D and -3D models. The dash line with the same color indicates the occurrence of preferential flow that is simulated. PF, preferential flow.

storage. The overland flow was simulated to be a relatively small portion of the rainfall and only occurred due to larger rainfall events at higher intensity (Figure S3).

The lateral water flows were well presented by both 3D and 2D models at catena and catchment scales. The 3D models predicted soil moisture content distributions considering convergent lateral flow lines, as demonstrated by the 3D simulated pressure heads in the example from August 20, 2007 (Figure 5). Intriguingly, the 2D model (simulation 4, assuming

the dual-porosity model and free drainage lower BC) clearly shows subsurface lateral flow pathways after rainfall events in terms of the flow velocity and the velocity vectors (Figure 6). In this example, subsurface lateral flow in the shallow Weikert soil (site 74) was simulated in the R horizon while in a deep soil such as the Rushtown (site 51), the subsurface lateral flow occurred in the B and C horizons (i.e., indicated with pink-red triangles in Figure 6). The nearly-saturated soil moisture content suggests that the water infiltrated into the bedrock

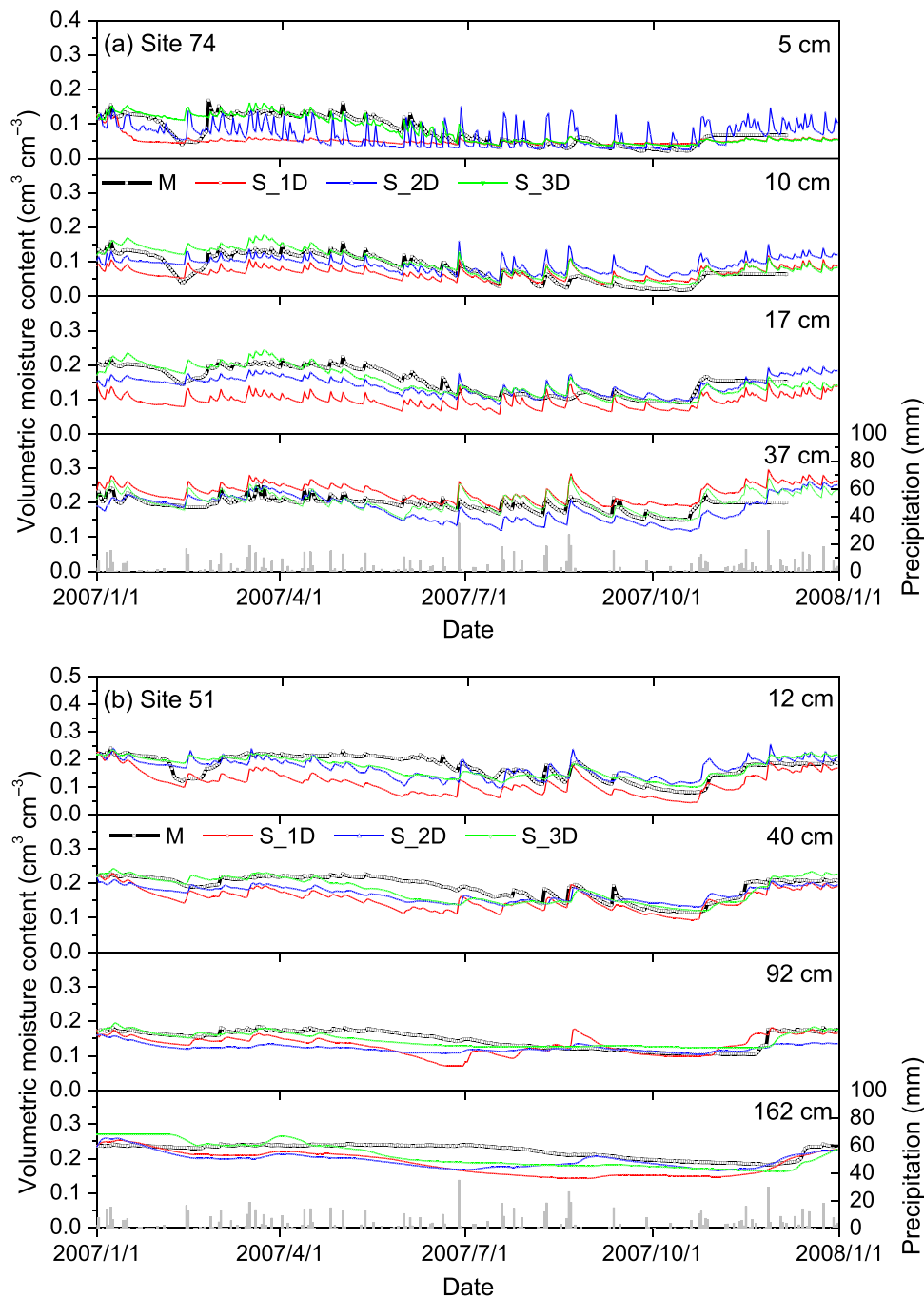


FIGURE 4 Time series of measured (M) and simulated soil moisture and rainfall intensities in 2007 at sites 74 (a) and 51 (b) by the HYDRUS-1D (S_1D), -2D (S_2D) and -3D (S_3D) models.

fractures below the shallow Weikert soil and moved laterally to the deep horizons of the deep Rushtown soil.

3.2 | Soil hydraulic models and effects of BCs

When comparing the model performance of the 2D simulations (Table 4), the single-porosity model (simulation 4) did not perform as well as the dual-porosity model (i.e., the

baseline simulation 1); however, the results of the baseline simulations improved when assuming an anisotropic K_s (simulation 5) further improves the simulation results (Table 4). Figure 7 shows that both single- and dual-porosity approaches reflected the soil moisture dynamics throughout a hydrological year, and that the dual-porosity model performed better than the single-porosity model. Moreover, improvements by assuming anisotropy of the K_s values (Figure 8) indicated that the soil along the slope was characterized by a

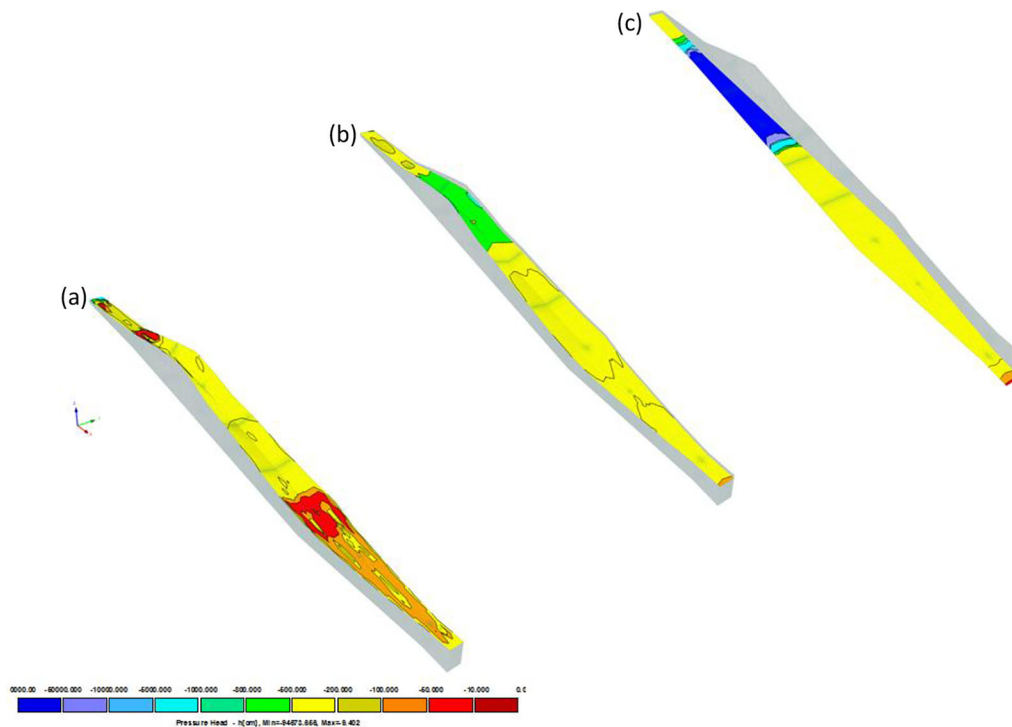


FIGURE 5 Snapshots of spatially variable pressure head at the 0-cm topsoil (a), the 40-cm subsoil (b), and the soil/bedrock interface (c) simulated by HYDRUS-3D for August 20, 2007.

vertically fractured or -macroporous (i.e., large K_v/K_h ratios) and horizontally platy or layered structure (i.e., large K_h/K_v ratios).

Regarding the bottom BCs, the use of a no flux BC (simulation 1) provided a better match of simulations with data than the use of a free drainage BC (simulation 6) at site 74 (Figure 9). In contrast, at site 51, a free drainage BC provided better predictions than a no flux BC (Figure 9). This differences in the goodness of fits (Table 4) suggested that site 74 was characterized by an impermeable subsurface layer and site 51 had a permeable soil-bedrock interface (Table 4).

The water table comparisons at site 15 in 2007 showed a similar dynamic of the simulated (simulation 3) and measured values (Figure 10), except for the summer period, when the simulations predicted a stronger water table drop than the measurements.

4 | DISCUSSION

4.1 | Identification of PF using a modeling approach

Our study indicated the occurrence of PF and lateral flow based on the analysis of soil moisture content dynamics (Figure 2), evaluated through numerical simulations using reasonable utilization of physically based models and cali-

brated hydraulic parameters (Figure 3). The PF occurrence was determined by both internal properties and external influences (Guo & Lin, 2018). The 1D hydrological models were challenged to simulate the PF (Figure 3) and often exhibited sequential flows (Larsson & Jarvis, 1999). In 2D simulations, the flow from ridges to valleys (Figure 6) was depicted, showcasing the interconnected nature of adjacent soil units where, according to Zepp et al. (2005), the lateral PF developed by connecting individual macropores into a “self-organized” network. In studies conducted at both pedon and hillslope scales, image analysis with dye tracers and X-ray computed tomography have highlighted the significant influence of surface topography in governing the process of PF (Mooney & Morris, 2008). The 3D simulations exhibited better performance than the 2D simulations, demonstrating the importance of the 3D models in the capture of lateral convergence, particularly in concave hillside positions (Figure 3b), which has been documented in previous observations (Graham & Lin, 2011). Despite past performance limitations of the 3D models in complex terrains (Loague et al., 2006; Mirus et al., 2007), our research underscores the importance of these simulations in the capture of PF dynamics and the more apparent lateral water flow within the area where the impermeable bedrock frequently occurred (Figure 9). Notably, while prior studies (Camporese et al., 2019; Hopp & McDonnell, 2009; James et al., 2010; Tromp-van Meerveld & Weiler, 2008) quantified hydrologic variables related to the PF, these studies did not

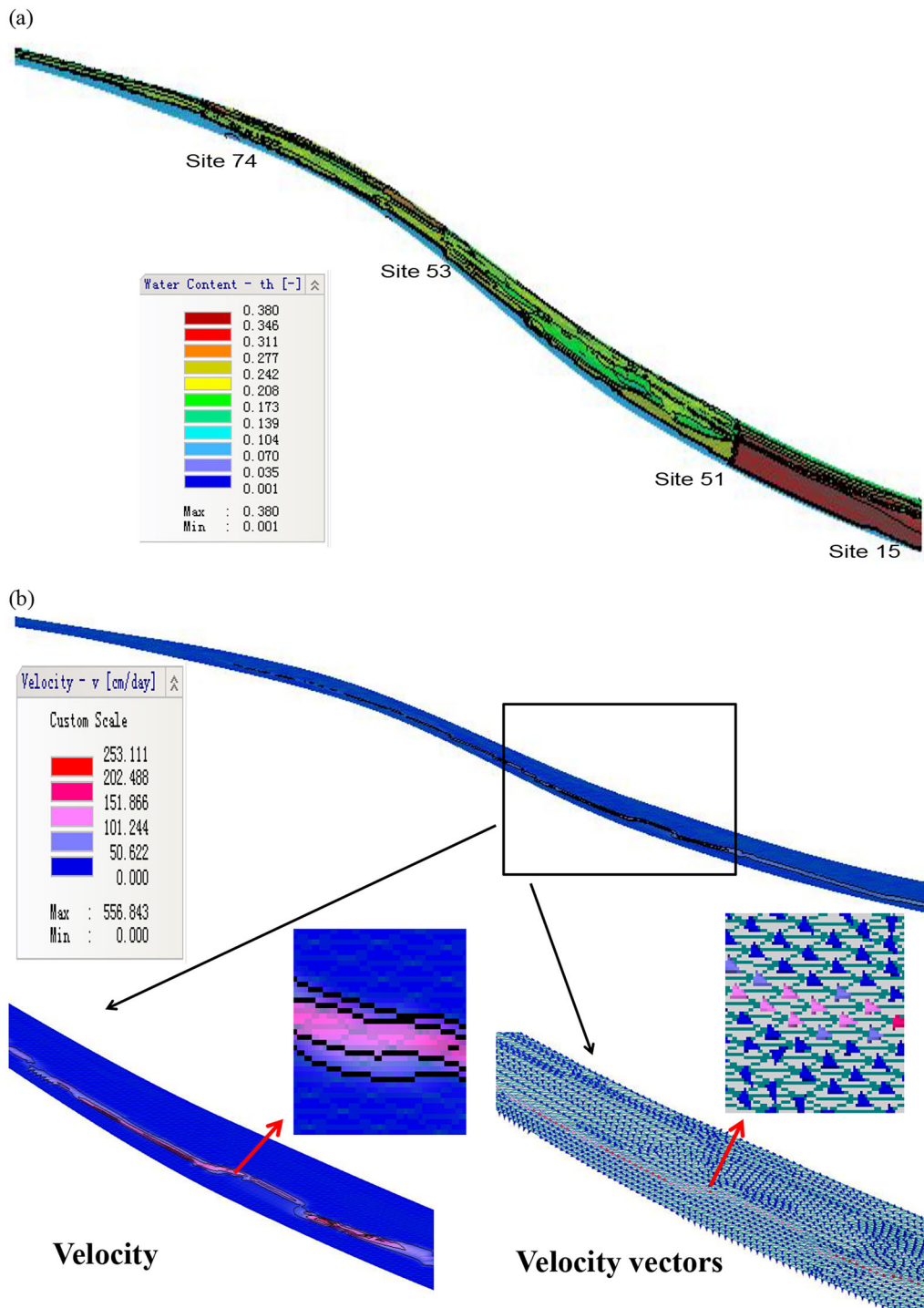


FIGURE 6 The 2D-distribution of (a) soil moisture content values and (b) water flux velocities displayed for August 20, 2007 (with the dual-porosity model and free drainage lower boundary).

always accurately simulate occurrence of PF, especially when compared to field observations.

Moving model from profile to larger scales necessitates accounting for spatially variable input conditions, soil properties, and geological factors, which was confirmed by our model approaches for representing PF effects in soils (Beven & Germann, 2013). Scaling knowledge from pedon to catch-

ment is challenging due to spatial variability and dynamic responses along the slope (Figure 2) with the increased significance of deeper flow pathways following slope positions (Beven & Germann, 2013; Tromp-van Meerveld et al., 2007; Vereecken et al., 2022). At hilltop site 74, the 3D simulations showed delays against the measured data (Figure 3), which may be potentially attributed to the water repellency often

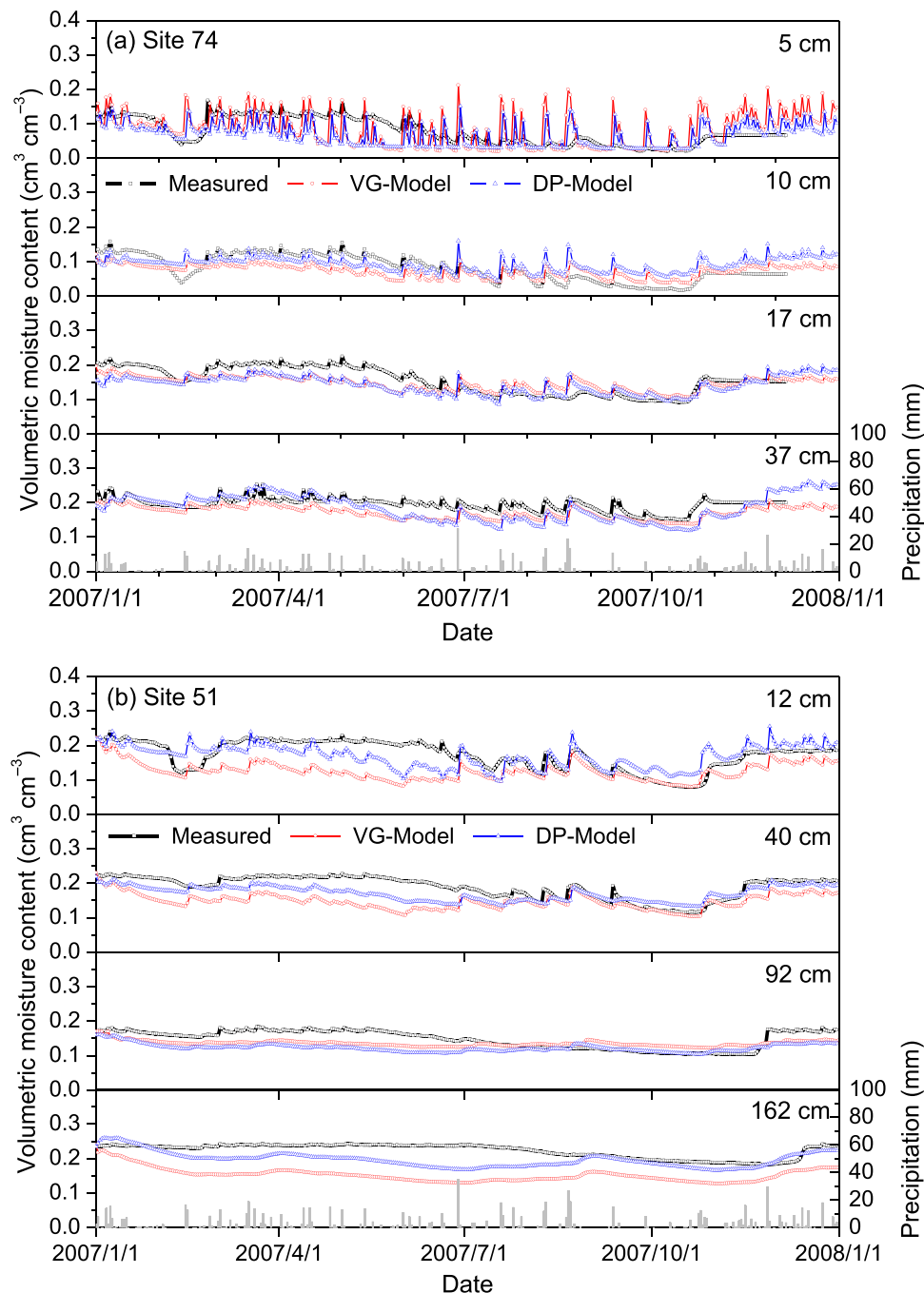


FIGURE 7 Comparisons between measured and simulated soil moisture in 2007 for the single-porosity model (VG) and the dual-porosity model (DP) at sites 74 (a) and 51 (b) for the HYDRUS-2D model.

associated with leaf litter accumulation or any lateral subsurface flow from an upslope area that was not adequately represented within our model domain (Lin et al., 2006; Lin & Zhou, 2008). Because site 74 is located near the peak of a hill, the short distance to the peak is crucial to produce a hydrological response (i.e., the threshold water pressure to activate PF) at a less permeable layer, such as an unweathered rock at the base of a profile. This potential situation (i.e., bedrock contributing area) underscores the need to revisit hillslope scale

responses in the context of water-initiated processes during wetting and drying events (Freer et al., 1997).

4.2 | Model complexities in simulating PF

Our studies found that the dual-porosity model described soil water flow processes better than the single-porosity model, which is consistent with other studies (e.g., Jarvis et al., 2016;

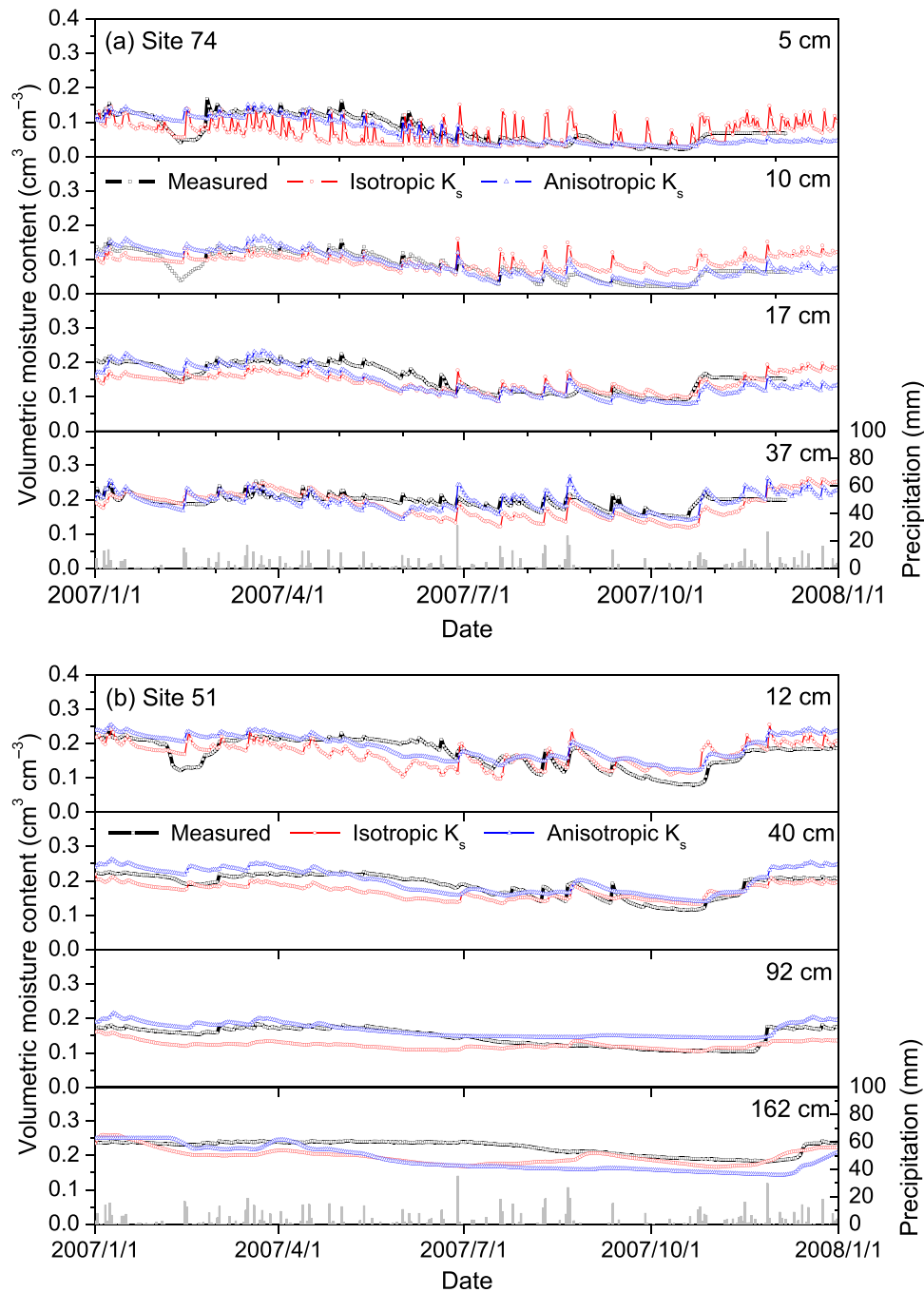


FIGURE 8 Comparisons between measured and predicted soil moisture values displayed over time in 2007 for isotropic saturated hydraulic conductivity (K_s) and anisotropic K_s at sites 74 (a) and 51 (b) by the HYDRUS-2D model.

Köhne et al., 2004; Šimůnek et al., 2003). Our findings support that dual-porosity models, considering the fracture-matrix structure of the soil, effectively capture soil moisture dynamics (Figure 7). In this scenario, microtopography's impact on vertical PF formation is evident (e.g., 3D simulation is better than 2D simulation; Figure 3). The accumulating hydraulic pressure in the depressions activates macropores, thereby directing the flow preferentially. Stratified soils often have greater horizontal than vertical K_s (Beckwith et al., 2003;

McCord et al., 1991; Newman et al., 1998), which was also found within the deep soil layers of the Shale Hills (Table 1). Doolittle et al. (2012) demonstrated that in our forested catchment with channery shale soils, lateral PF occurred along the bedding planes in the fractured shale. Guo et al. (2019) also noted that water movement in the study area aligns with the lateral slope, especially in the deeper soil. This observation could help clarify why simulations with anisotropic K_s values were more accurate than those assuming isotropic K_s

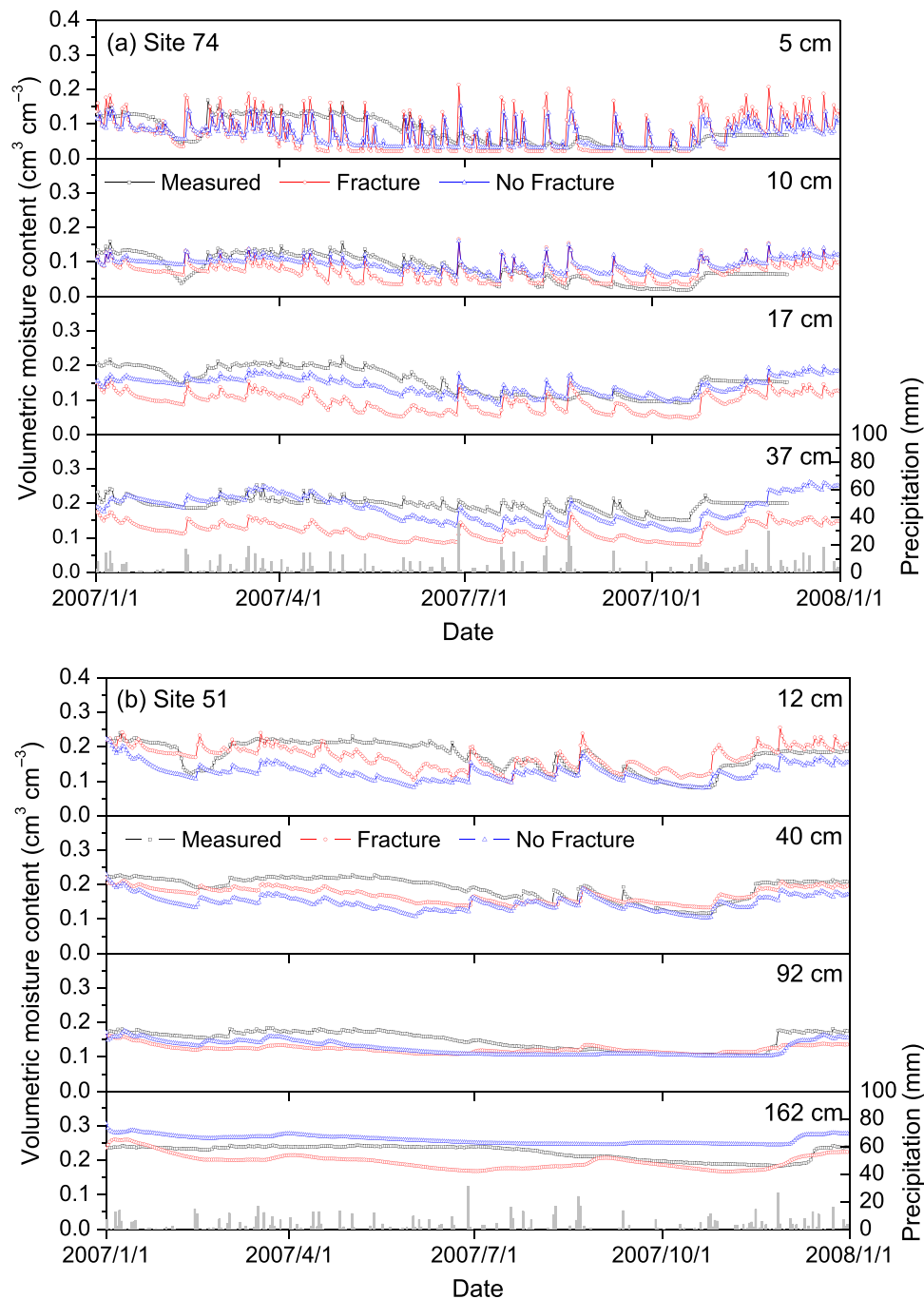


FIGURE 9 Comparisons between measured and simulated soil moisture values in 2007 for permeable free drainage boundary condition (fracture) and impermeable no-flux boundary condition (no fracture) for sites 74 (a) and 51 (b) by the HYDRUS-2D model.

(Figure 8). Omitting anisotropy in hydraulic parameters can even skew results (Ebel et al., 2007; James et al., 2010). The implication is that anisotropic K_s more accurately represent impacts of rock fragments and fissures, with the studied watershed marked by both weathered and unweathered bedrocks facilitating lateral flow.

Our study emphasizes to accurately represent fractured shale geology when simulating PF occurrence. While numerical models often view bedrock as impermeable, evidence

suggests bedrock may sometimes be more or less permeable (Camporese et al., 2019). Modeling requires considering both permeable fracture-structured shale bedrock and less or impermeable bedrock (Figure 9). Ebel et al. (2007) highlighted prediction errors when layered geological interfaces are misrepresented. For instance, minor errors in simulating soil water contents can lead to significant discrepancies in perched water depths (Lin et al., 2006). The 3D model performance may be enhanced by detailed geological

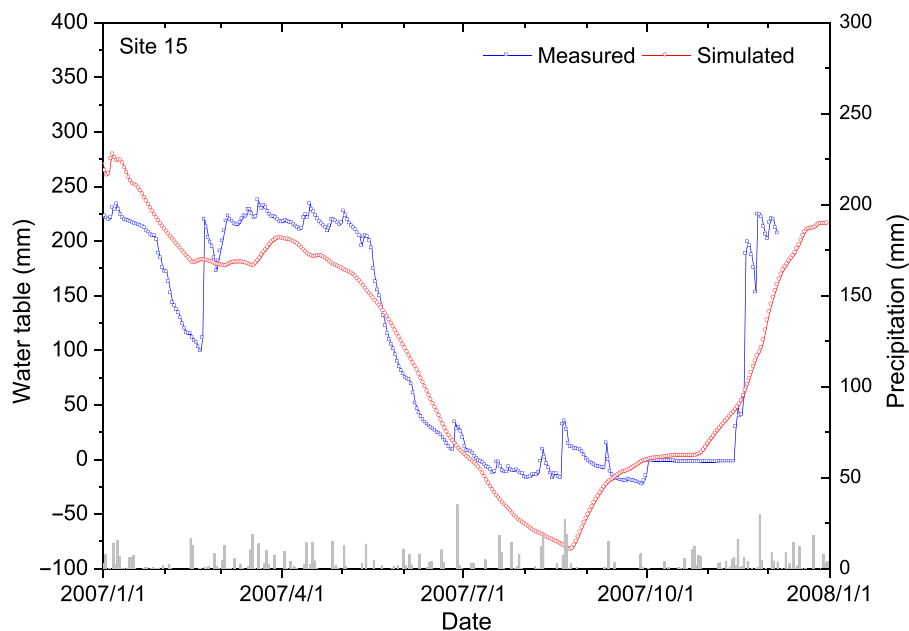


FIGURE 10 Comparisons between measured and simulated water tables for site 15 with precipitation distribution as a reference.

characterization to improve predictions (Figures 5 and 6), as continuous parameterization of sub-catchment structures remains a challenge. Beven and Germann (2013) noted the difficulty in determining site-specific soil characteristics regardless of the flow process representation used (e.g., site 74; Figure 3).

4.3 | Flow pathways and connectivities along the hillslope

High-resolution soil moisture monitoring identified PF occurrence in the 1D vertical profile (Figure 2). Combined with a 2/3D model analysis, hillslope-scale flow patterns can be discerned in our study. Few rainfall events during our study created fast water flow from hilltop to valley positions despite PF detection at each site (see Figure 2). Similarly, Sidle et al. (2001) also found that when forested soils reached a certain threshold water pressure, macropores became more hydraulically active. This occurrence led to the development of an expanded macropore network, which in turn enhanced the effective conductance of these soils. During rainstorms (e.g., 10 mm h^{-1} ; Figure 3) with initially dry soil, vertical macropore flow combined with lateral matrix flow was more evident in concave midslope, while planar uphill saw dominant lateral subsurface flow (Figure 7). These results may suggest that flow paths were “locally” connected in dry conditions but could extend to the valley (Guo et al., 2014), as seen in our 3D simulations (Figure 5). A perched water table’s development (Guo et al., 2014) likely spurred downslope subsurface water movement, marked by topsoil moisture surges post-large rains

at site 15 (Figure 10). This perched water table suggests vertical K_s value restrictions in lower soil layers (Table 2), leading to gravity-driven flow. Water was then channeled laterally to high-permeability zones, flowing to the catchment’s outlet.

Multidimensional modeling improved our understanding of hillslope hydrology, such as flow path connectivity (Salve et al., 2012). Two subsurface lateral flow paths were identified: one related to soil structure and another to subsurface fractures. The first pathway started upslope (Figure 11, left) where rainwater could infiltrate rapidly, met a less permeable bedrock, and then moved laterally, recharging the Bw and C horizons downslope (Guo et al., 2014). This observation aligns with the findings of Haria et al. (2003), who observed an increased occurrence of PF at the interface between soil and bedrock in shallow soils above fissured chalk, particularly when the water table is close to the surface. A second pathway occurred when water flowed through bedrock fractures, recharged the deep C horizon downslope (Figure 11, right), and facilitated rapid lateral flow above the groundwater, especially during wet conditions and sustained rainfall. Since drainage toward deeper layers was restricted along the midslope by the relatively impermeable subsurface horizons (Figures 5 and 6), soil water could enter the subsurface mainly in a downslope region. In the valley floor area (at site 15), there was likely significant water interactions (e.g., water table dynamics; Figure 10) occurring between the fractured bedrocks above and beneath an embedded clay layer (Table 2). Simulated water table deviations from measurements may be caused by inadequate consideration of a perched water table and subsequent groundwater recharge into the soil. Nonetheless, the comparable patterns and behaviors observed suggest

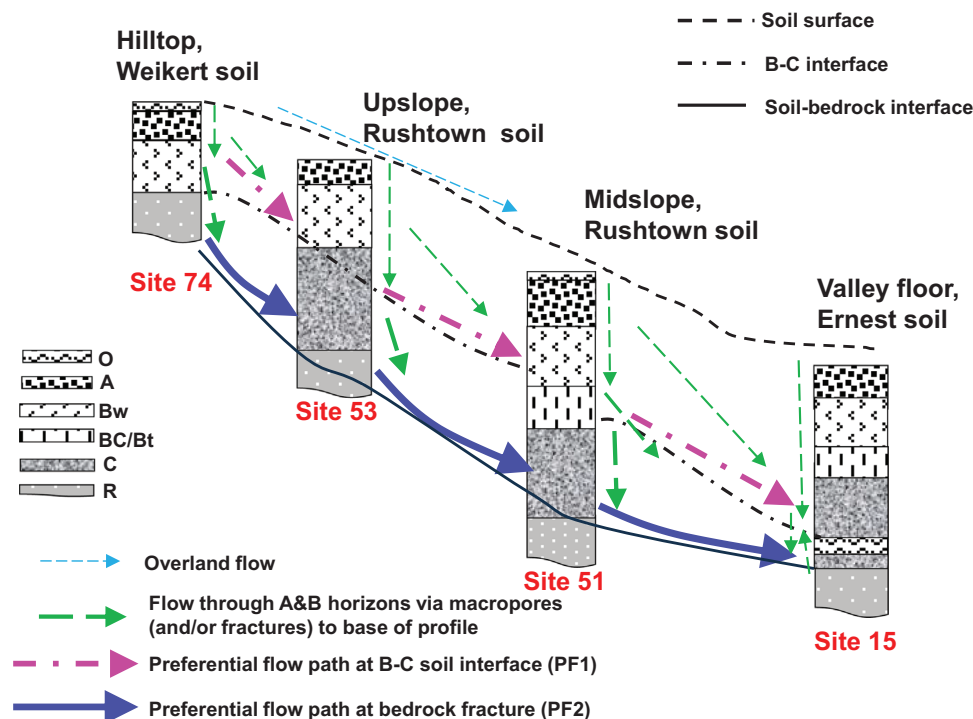


FIGURE 11 Conceptual diagram showing several potential subsurface preferential flow pathways along a hillslope in the Shale Hills catchment. The soil series and soil horizons are indicated for each landscape positions (see in Table 1).

that our model may have captured the dynamics of lateral subsurface drainage moving from hilltops to valleys.

4.4 | Evaluation of the model performance

Based on the monitoring evidence of PF and the hillslope's soil hydraulic and geomorphological conditions, 2/3D modeling results (Figure 6) confirmed that subsurface lateral flow is a vital flow mechanism along slopes of the Shale Hill catchment (Lin et al., 2006). The simulations demonstrated that Richards' equation-based numerical models can help analyze and identify subsurface lateral and PF paths (Figure 11, conceptual scheme). Considering the complexity and refinement of 2D and 3D "bottom-up" physically based models in illustrating variations in soil profiles at a larger scale, our research has the potential to significantly contribute to creating a comprehensive modeling framework.

Compared to earlier studies (Fan et al., 2019), our evaluation and suggested scheme (Figure 11) provides a more quantitative understanding of how smaller soil structural processes affect larger scale hydrological flows (Beven et al., 2020; Vereecken et al., 2022); this is because of a more extensive dataset for calibration and validation (Figures S1 and S2). Our 3D simulations, beyond capturing 1D vertical and 2D anisotropic soil water movement, also depict the spatial distribution of soil types and flow path convexity on the hillslope (Figure 5) as noted by Camporese et al. (2019). Consequently,

the model discretization captured micro-topography worked much better than the model that did not account for those smaller spatial features.

The 3D model illustrates the subsurface as a spatial continuum of soil horizons that are slope oriented layered soil bedrock (Figure 1), integrating the small-scaled spatially variable soil hydrological properties (Rakovec et al., 2016). This layered structure (Table 1), which considered the importance of the often-overlooked anisotropic hydraulic conductivity, improved the present hydrological simulations (see Figure 8) with results similar to a previous study (McDonnell et al., 2007). While direct field methods to evaluate soil anisotropy and bedrock permeability effects are absent (Camporese et al., 2019; James et al., 2010), the present model-based analyses (Figures 8 and 9) improved the results considerably in terms of smaller RMSE and higher NSE values (Table 4). The assumption of varying bottom BC permeability enhances simulations by considering soil-bedrock interactions in forested hillslopes with potential fractures (see Figure 9), similar to previous studies (Camporese et al., 2019).

Our model approaches confirmed that the Richards equation-based numerical code HYDRUS can simulate a physical representation of the PF process, although the presence of this inclusion has frequently been questioned (e.g., Beven, 2018). Camporese et al. (2019) and Beven and German (2013) used the Richards equation-based numerical model (CATHY) to generate a threshold-driven hillslope response, such as the fill-and-spill mechanism at Panola Mountain

TABLE 4 Nash–Sutcliffe efficiency (NSE) values and root mean square errors (RMSE) of the 1D, 2D, and 3D modeling approaches during the hydrological year 2007 at the sites 74 and 51 as used in the dual-porosity model (DP), impermeable bedrock (IB), and isotropy K_s at the pedon scale.

Site	Soil depth (cm)	Simulation using the single-porosity model (VG), impermeable bedrock (IB) and isotropic K_s									Alternate versions of the 2D model								
		NSE			RMSE			3D			2D			NSE			RMSE		
		ID	2D	3D	3D	2D	3D	3D	2D	3D	DP	FB	Ani	DP	FB	Ani			
74	5	-0.319	0.122	0.705	0.045	0.021	0.021	0.021	0.020	0.020	-0.153	-0.282	0.220	0.020	0.050	0.023			
	10	0.169	0.399	0.737	0.035	0.024	0.020	0.020	0.020	0.296	0.329	0.360	0.018	0.031	0.018				
	17	-2.047	0.534	0.646	0.068	0.020	0.023	0.023	0.020	0.623	0.456	-2.223	0.017	0.029	0.18				
	37	-2.538	-0.195	-0.087	0.036	0.021	0.020	0.020	0.021	0.475	-1.330	-16.823	0.017	0.029	0.019				
51	12	-1.562	-1.026	0.312	0.067	0.059	0.034	0.034	0.059	0.239	0.498	-0.256	0.036	0.030	0.049				
	40	-0.627	-0.307	0.439	0.042	0.050	0.025	0.025	0.050	0.191	0.516	-0.127	0.029	0.023	0.040				
	92	-0.441	0.017	0.222	0.032	0.026	0.023	0.023	0.026	0.128	0.567	0.036	0.024	0.015	0.021				
	162	-3.790	-2.558	-3.448	0.044	0.074	0.043	0.043	0.074	-2.015	-0.676	-2.874	0.035	0.026	0.040				

Note: The comparisons included the corresponding 2D simulations of the single-porosity model (VG), fractured bedrock (FB), and anisotropy K_s (Ani). A bold number means good model performance.

Research Watershed. Hopp and McDonnell (2009) earlier confirmed that the Richards equation-based numerical code HYDRUS can simulate the fill-and-spill mechanism.

A conceptual fill-and-spill model of subsurface runoff generation (Guo et al., 2019) supported the model interpretation and conceptual development (Figure 11) used in our study. The present iteration of studying hillslope hydrological processes (i.e., at Shale Hills) links understanding, data, and modeling (Grayson & Blöschl, 2000). The field validation of physical-based models, although still limited, have already allowed the identification of fractured bedrock flow (Figure 9) as an essential process (Beven et al., 2020). With more detailed information on the subsurface (e.g., soil horizons, macropores, and bedrock) obtained through the use of ground penetrating radar and/or electrical resistivity tomography techniques (Guo & Lin, 2018), it has been postulated that an appropriately parameterized, physical-based model will be able to simulate catchment-scale water flow (Fan et al., 2019).

5 | CONCLUSIONS

We compared simulations of increasingly complex models with consistent soil moisture datasets. The multidimensional modeling aimed to elucidate how soil-landscape features in a small catchment affect subsurface lateral and vertical PF processes. The comparison of simulations with 1D, 2D, and 3D numerical models was conducted to evaluate the effects of considering relevant processes and BCs. The model results confirmed that better representation in model parameterization generally improves accuracy. The detailed characterization of shale-derived soil thickness in a 3D representation was found to be critical for the simulation of the pore-water pressure and convergent subsurface flow at catchments like the Shale Hills. Results further suggested that (1) the inclusion of PF generally improved the predictions regardless of the model dimension (1D, 2D, or 3D) being used, (2) the dual-porosity model outperformed the single-porosity model since it helped estimating the contributions of macropore flow within the soil, (3) the consideration of anisotropic K_s generally also improved the model accuracy, and (4) the models that considered the presence of fractured bedrock performed better than those models that neglected fractures within the bedrock as a BC.

AUTHOR CONTRIBUTIONS

Ying Zhao: Conceptualization; data curation; formal analysis; funding acquisition; investigation; methodology; resources; software; supervision; validation; visualization; writing—original draft; writing—review and editing. **Jun Yi:** Data curation; methodology; writing—original draft. **Rongjiang Yao:** Methodology; software. **Fei Li:** Conceptualization; resources. **Robert Lee Hill:** Conceptualization;

supervision; validation; writing—review and editing. **Horst H. Gerke**: Conceptualization; supervision; validation; writing—review and editing.

ACKNOWLEDGMENTS

This research was backed by the U.S. NSF via the Shale Hills CZO grant (PI: H. Lin; EAR-1416881), the National Natural Science Foundation of China (42320104006), and Taishan Scholars Program (201812096, 202211185). Fei Li and Robert Lee Hill received support from the CAAS-ASTIP-2020-IGR-04 and the USDA National Institute of Food and Agriculture, Hatch project (grant nos. 1014496), respectively. Data came from the NSF's Southern Sierra CZO, available at <http://criticalzone.org/shale-hills/data/datasets/>. Thanks to the Penn State Hydrogeology Group, M. Flury (Washington State University), and J. J. McDonnell (University of Saskatchewan) for their contributions.

CONFLICT OF INTEREST STATEMENT

The authors declare no conflicts of interest.

ORCID

Ying Zhao  <https://orcid.org/0000-0003-0346-5631>

REFERENCES

- Beckwith, C. W., Baird, A. J., & Heathwaite, A. L. (2003). Anisotropy and depth-related heterogeneity of hydraulic conductivity in a bog peat. II: Modelling the effects on groundwater flow. *Hydrological Processes*, *17*, 103–113. <https://doi.org/10.1002/hyp.1117>
- Beven, K. (2018). A century of denial: Preferential and nonequilibrium water flow in soils. *Vadose Zone Journal*, *17*, 1–17. <https://doi.org/10.2136/vzj2018.08.0153>
- Beven, K., Asadullah, A., Bates, P., Blyth, E., Chappell, N., Child, S., Cloke, H., Dadson, S., Everard, N., Fowler, H. J., Freer, J., Hannah, D. M., Heppell, K., Holden, J., Lamb, R., Lewis, H., Morgan, G., Parry, L., & Wagener, T. (2020). Developing observational methods to drive future hydrological science: Can we make a start as a community? *Hydrological Processes*, *34*, 868–873. <https://doi.org/10.1002/hyp.13622>
- Beven, K., & Germann, P. (1982). Macropores and water flow in soils. *Water Resources Research*, *18*, 1311–1325. <https://doi.org/10.1029/WR018i005p01311>
- Beven, K., & Germann, P. (2013). Macropores and water flow in soils revisited. *Water Resources Research*, *49*, 3071–3092. <https://doi.org/10.1002/wrcr.20156>
- Bittelli, M., Tomei, F., Pistorcchi, A., Flury, M., Boll, J., Brooks, E. S., & Antolini, G. (2010). Development and testing of a physically based, three-dimensional model of surface and subsurface hydrology. *Advance in Water Resources*, *33*, 106–122. <https://doi.org/10.1016/j.advwatres.2009.10.013>
- Blöschl, G., & Grayson, R. B. (2001). *Spatial patterns in catchment hydrology: Observations and modelling*. Cambridge University Press.
- Brantley, S. L., White, T., West, N., Williams, J. Z., Forsythe, B., Shapich, D., Kaye, J., Lin, H., Shi, Y., Kaye, M., & Herndon, E. (2018). Susquehanna Shale Hills critical zone observatory: Shale Hills in the context of Shaver's Creek watershed. *Vadose Zone Journal*, *17*(1), 1–19. <https://doi.org/10.2136/vzj2018.04.0092>
- Buttle, J. M., & McDonald, D. J. (2002). Coupled vertical and lateral preferential flow on a forested slope. *Water Resources Research*, *38*, 18-1–18-16. <https://doi.org/10.1029/2001WR000773>
- Camporese, M., Paniconi, C., Putti, M., & McDonnell, J. J. (2019). Fill and spill hillslope runoff representation with a Richards equation-based model. *Water Resources Research*, *55*, 8445–8462. <https://doi.org/10.1029/2019WR025726>
- Clark, M. P., Fan, Y., Lawrence, D. M., Adam, J. C., Bolster, D., Gochis, D. J., Hooper, R. P., Kumar, M., Leung, L. R., Mackay, D. S., Maxwell, R. M., Shen, C., Swenson, S. C., & Zeng, X. (2015). Improving the representation of hydrologic processes in Earth System Models. *Water Resources Research*, *51*, 5929–5956. <https://doi.org/10.1002/2015WR017096>
- Clothier, B. E., Heng, L., Magesan, G. N., & Vogeler, I. (1995). The measured mobile-water content of an unsaturated soil as a function of hydraulic regime. *Australian Journal of Soil Research*, *33*, 397–414. <https://doi.org/10.1071/SR950397>
- Doolittle, J., Zhu, Q., Zhang, J., Guo, L., & Lin, H. (2012). Geophysical investigations of soil landscape architecture and its impacts on subsurface flow. In H. Lin (Ed.), *Hydrogeology: Synergistic integration of soil science and hydrology* (pp. 413–447) Academic Press, Elsevier.
- Durner, W. (1994). Hydraulic conductivity estimation for soils with heterogeneous pore structure. *Water Resources Research*, *30*, 211–233. <https://doi.org/10.1029/93WR02676>
- Dusek, J., & Vogel, T. (2014). Modeling subsurface hillslope runoff dominated by preferential flow: One- vs. two-dimensional approximation. *Vadose Zone Journal*, *13*, 1–13. <https://doi.org/10.2136/vzj2013.05.0082>
- Ebel, B. A., Loague, K., Vanderkwaak, J. E., Dietrich, W. E., Montgomery, D. R., Torres, R., & Anderson, S. P. (2007). Near-surface hydrologic response for a steep, unchanneled catchment near Coos Bay, Oregon: 2. Physics-based simulations. *American Journal of Science*, *307*, 709–748. <https://doi.org/10.2475/04.2007.03>
- Fan, Y., Clark, M., Lawrence, D. M., Swenson, S., Band, L. E., Brantley, S. L., Brooks, P. D., Dietrich, W. E., Flores, A., Grant, G., Kirchner, J. W., Mackay, D. S., McDonnell, J. J., Milly, P. C. D., Sullivan, P. L., Tague, C., Ajami, H., Chaney, N., Hartmann, A., ... Yamazaki, D. (2019). Hillslope hydrology in global change research and Earth System Modeling. *Water Resources Research*, *55*, 1737–1772. <https://doi.org/10.1029/2018WR023903>
- Feddes, R. A., Kowalik, P. J., & Zaradny, H. (1978). *Simulation of field water use and crop yield*. John Wiley and Sons.
- Freer, J., McDonnell, J. J., Beven, K. J., Brammer, D., Burns, D., Hooper, R. P., & Kendall, C. (1997). Topographic controls on subsurface storm flow at the hillslope scale for two hydrologically distinct small catchments. *Hydrological Processes*, *11*, 1347–1352. [https://doi.org/10.1002/\(SICI\)1099-1085\(199707\)11:9<1347::AID-HYP592>3.0.CO;2-R](https://doi.org/10.1002/(SICI)1099-1085(199707)11:9<1347::AID-HYP592>3.0.CO;2-R)
- Freeze, R. A. (1972). Role of subsurface flow in generating surface runoff I. Base flow contributions to channel flow. *Water Resources Research*, *8*, 609–624. <https://doi.org/10.1029/WR008i003p00609>
- Gao, M., Li, H.-Y., Liu, D., Tang, J., Chen, X., Chen, X., Blöschl, G., & Leung, L. R. (2018). Identifying the dominant controls on macropore flow velocity in soils: A meta-analysis. *Journal of Hydrology*, *567*, 590–604. <https://doi.org/10.1016/j.jhydrol.2018.10.044>
- Gardenas, A. I., Šimůnek, J., Jarvis, N., & van Genuchten, M. Th. (2006). Two-dimensional modelling of preferential water flow and pesticide transport from a tile-drain field. *Journal of Hydrology*, *329*, 647–660. <https://doi.org/10.1016/j.jhydrol.2006.03.021>

- Gerke, H. H., Germann, P. F., & Nieber, J. (2010). Preferential and unstable flow: From the pore to the catchment scale. *Vadose Zone Journal*, 9, 207–212. <https://doi.org/10.2136/vzj2010.0059>
- Gerke, H. H., & van Genuchten, M. Th. (1993a). A dual-porosity model for simulating the preferential movement of water and solutes in structured porous media. *Water Resources Research*, 29, 305–319. <https://doi.org/10.1029/92WR02339>
- Gerke, H. H., & van Genuchten, M. Th. (1993b). Evaluation of a first order water transfer term for variably saturated dual-porosity flow models. *Water Resources Research*, 29, 1225–1238. <https://doi.org/10.1029/92WR02467>
- Graham, C., & Lin, H. S. (2011). Controls and frequency of preferential flow occurrence at the Shale Hills Critical Zone Observatory: A 175 event analysis of soil moisture response to precipitation. *Vadose Zone Journal*, 10, 816–831. <https://doi.org/10.2136/vzj2010.0119>
- Grayson, R., & Blöschl, G. (Eds.). (2000). *Spatial modelling of catchment dynamics*. In *Spatial patterns in catchment hydrology: Observations and modelling*. (pp. 51–58). Cambridge University Press.
- Gu, W. Z., Liu, J. F., Lin, H. S., Lin, J., Liu, H. W., Liao, A.-M., Wang, N., Wang, W. Z., Ma, T., Yang, N., Li, X. G., Zhuo, P., & Cai, Z. (2018). Why hydrological maze: The hydro-pedological trigger? Review of experiments at Chuzhou Hydrology Laboratory. *Vadose Zone Journal*, 17, 170174. <https://doi.org/10.2136/vzj2017.09.0174>
- Guo, L., & Lin, H. (2018). Addressing two bottlenecks to advance the understanding of preferential flow in soils. *Advances in Agronomy*, 147, 61–117. <https://doi.org/10.1016/bs.agron.2017.10.002>
- Guo, L., Lin, H., Fan, B., Nyquist, J., Toran, L., & Mount, G. (2019). Preferential flow through shallow fractured bedrock and a 3D fill-and-spill model of hillslope subsurface hydrology. *Journal of Hydrology*, 576, 430–442. <https://doi.org/10.1016/j.jhydrol.2019.06.070>
- Guo, L., Lin, H. S., & Chen, J. (2014). Subsurface lateral flow network on a hillslope revealed by time-lapse ground penetrating radar. *Water Resources Research*, 50, 9127–9147. <https://doi.org/10.1002/2013WR014603>
- Haga, H., Matsumoto, Y., Matsutani, J., Fujita, M., Nishida, K., & Sakamoto, Y. (2005). Flow paths, rainfall properties, and antecedent soil moisture controlling lags to peak discharge in a granitic unchanneled catchment. *Water Resources Research*, 41, W12410. <https://doi.org/10.1029/2005WR004236>
- Hargreaves, G. H., & Samani, Z. A. (1985). Reference crop evapotranspiration from temperature. *Applied Engineering In Agriculture*, 1(2), 96–99. <https://doi.org/10.13031/2013.26773>
- Haria, A. H., Hodnett, M. G., & Johnson, A. C. (2003). Mechanisms of groundwater recharge and pesticide penetration to a chalk aquifer in southern England. *Journal of Hydrology*, 275, 122–137. [https://doi.org/10.1016/S0022-1694\(03\)00017-9](https://doi.org/10.1016/S0022-1694(03)00017-9)
- Hendrickx, J. M. H., & Flury, M. (2001). Uniform and preferential flow, mechanisms in the vadose zone. In *Conceptual models of flow and transport in the fractured vadose zone* (pp. 149–187). National Research Council, National Academy Press.
- Hopp, L., & McDonnell, J. J. (2009). Connectivity at the hillslope scale: Identifying interactions between storm size bedrock permeability, slope angle and soil depth. *Journal of Hydrology*, 376, 378–391. <https://doi.org/10.1016/j.jhydrol.2009.07.047>
- James, A. L., McDonnell, J. J., Tromp-van Meerveld, I., & Peters, N. E. (2010). Gypsies in the palace: Experimentalist's view on the use of 3-D physics-based simulation of hillslope hydrological response. *Hydrological Processes*, 24, 3878–3893. <https://doi.org/10.1002/hyp.7819>
- Jarvis, N., Koestel, J., & Larsbo, M. (2016). Understanding preferential flow in the vadose zone: Recent advances and future prospects. *Vadose Zone Journal*, 15, 1–11. <https://doi.org/10.2136/vzj2016.09.0075>
- Jiang, Y., Zhang, Y., Fan, B., Wen, J., Liu, H., Mello, C. R., Cui, J., Yuan, C., & Guo, L. (2023). Preferential flow influences the temporal stability of soil moisture in a headwater catchment. *Geoderma*, 437, 116590. <https://doi.org/10.1016/j.geoderma.2023.116590>
- Kohne, J. M., Mohanty, B., Šimůnek, J., & Gerke, H. H. (2004). Numerical evaluation of a second-order water transfer term for variably saturated dual-permeability models. *Water Resources Research*, 40, W07409. <https://doi.org/10.1029/2004WR003285>
- Korres, W., Reichenau, T. G., Fiener, P., Koyama, C. N., Bogen, H. R., Cornelissen, T., Baatz, R., Herbst, M., Diekkrüger, B., Vereecken, H., & Schneider, K. (2015). Spatio-temporal soil moisture patterns: A meta-analysis using plot to catchment scale. *Journal of Hydrology*, 520, 326–341. <https://doi.org/10.1016/j.jhydrol.2014.11.042>
- Larsson, M. H., & Jarvis, N. J. (1999). Evaluation of a dual-porosity model to predict field-scale solute transport in a macroporous soil. *Journal of Hydrology*, 215, 153–171. [https://doi.org/10.1016/S0022-1694\(98\)00267-4](https://doi.org/10.1016/S0022-1694(98)00267-4)
- Lin, H. S., Kogelmann, W., Walker, C., & Bruns, M. A. (2006). Soil moisture patterns in a forested catchment: A hydro-pedological perspective. *Geoderma*, 131(3-4), 345–368.
- Lin, H., & Zhou, X. (2008). Evidence of preferential flow using soil hydrologic monitoring in the Shale Hills catchment. *European Journal of Soil Science*, 59, 34–49. <https://doi.org/10.1111/j.1365-2389.2007.00988.x>
- Liu, H., & Lin, H. S. (2015). Frequency and control of preferential flow: From pedon to catchment scales. *Soil Science Society of America Journal*, 79, 362–377. <https://doi.org/10.2136/sssaj2014.08.0330>
- Loague, K., Heppner, C. S., Mirus, B. B., Ebel, B. A., Ran, Q., Carr, A. E., BeVillie, S. H., & VanderKwaak, J. E. (2006). Physics-based hydrologic-response simulation: Foundation for hydroecology and hydrogeomorphology. *Hydrological Processes*, 20(5), 1231–1237. <https://doi.org/10.1002/hyp.6179>
- Loos, C., Gayler, S., & Priesack, S. (2007). Assessment of water balance simulations for large scale weighing lysimeters. *Journal of Hydrology*, 335, 259–270. <https://doi.org/10.1016/j.jhydrol.2006.11.017>
- Maxwell, R. M., & Kollet, S. J. (2008). Interdependence of groundwater dynamics and land-energy feedbacks under climate change. *Nature Geoscience*, 1, 665–669. <https://doi.org/10.1038/ngeo315>
- McCord, J. T., Stephens, D. B., & Wilson, J. L. (1991). Hysteresis and state-dependent anisotropy in modeling unsaturated hill slope hydrologic processes. *Water Resources Research*, 27, 1501–1518. <https://doi.org/10.1029/91WR00880>
- McDonnell, J. J., Sivapalan, M., Vaché, K., Dunn, S. M., Grant, G., Haggerty, R., Hinz, C., Hooper, R., Kirchner, J., Roderick, M. L., Selker, J., & Weiler, M. (2007). Moving beyond heterogeneity and process complexity: A new vision for watershed hydrology. *Water Resources Research*, 43, W07301. <https://doi.org/10.1029/2006WR005467>
- Melsen, L. A., Teuling, A. J., Torfs, P. J. J. F., Uijlenhoet, R., Mizukami, N., & Clark, M. P. (2016). HESS Opinions: The need for process-based evaluation of large-domain hyper-resolution models. *Hydrology and Earth System Sciences*, 20, 1069–1079. <https://doi.org/10.5194/hess-20-1069-2016>
- Mirus, B. B., Ebel, B. A., Loague, K., & Wemple, B. C. (2007). Simulated effect of a forest road on near-surface hydrologic response:

- Redux. *Earth Surface Processes and Landforms*, 32(1), 126–142. <https://doi.org/10.1002/esp.1387>
- Mooney, S. J., & Morris, C. (2008). Morphological approach to understanding preferential flow using image analysis with dye tracers and X-ray computed tomography. *Catena*, 73, 204–211. <https://doi.org/10.1016/j.catena.2007.09.003>
- Newman, B. D., Campbell, A. R., & Wilcox, B. P. (1998). Lateral subsurface flow pathways in a semiarid ponderosa pine hillslope. *Water Resources Research*, 34, 3485–3496. <https://doi.org/10.1029/98WR02684>
- Nimmo, J. R. (2012). Preferential flow occurs in unsaturated conditions. *Hydrological Processes*, 26, 786–789. <https://doi.org/10.1002/hyp.8380>
- Noguchi, S., Tsuboyama, Y., Sidle, R. C., & Hosoda, I. (1999). Morphological characteristics of macropores and the distribution of preferential flow pathways in a forested slope segment. *Soil Science Society of America Journal*, 63, 1413–1423. <https://doi.org/10.2136/sssaj1999.6351413x>
- Rakovec, O., Kumar, R., Attinger, S., & Samaniego, L. (2016). Improving the realism of hydrologic model functioning through multivariate parameter estimation. *Water Resources Research*, 52, 7779–7792. <https://doi.org/10.1002/2016WR019430>
- Saito, H., Šimůnek, J., & Mohanty, B. P. (2006). Numerical analysis of coupled water, vapor, and heat transport in the vadose zone. *Vadose Zone Journal*, 5, 784–800. <https://doi.org/10.2136/vzj2006.0007>
- Salve, R., Rempe, D. M., & Dietrich, W. E. (2012). Rain, rock moisture dynamics, and the rapid response of perched groundwater in weathered, fractured argillite underlying a steep hillslope. *Water Resources Research*, 48, 1–25. <https://doi.org/10.1029/2012WR012583>
- Scanlon, B. R., Christman, M., Reedy, R., Porro, I., Šimůnek, J., & Flerchinger, G. (2002). Intercode comparisons for simulating water balance of surficial sediments in semiarid regions. *Water Resources Research*, 38, 59–1–59–16. <https://doi.org/10.1029/2001WR001233>
- Schulz, K., Seppelt, R., Zehe, E., Vogel, H. J., & Attinger, S. (2006). Importance of spatial structures in advancing hydrological sciences. *Water Resources Research*, 42, W03S03. <https://doi.org/10.1029/2005WR004301>
- Sidle, R., Noguchi, S., Tsuboyama, Y., & Laursen, K. (2001). A conceptual model of preferential flow systems in forested hillslopes: Evidence of self-organization. *Hydrological Processes*, 15, 1675–1692. <https://doi.org/10.1002/hyp.233>
- Šimůnek, J., van Genuchten, M. Th., & Sejna, M. (2016). Recent developments and applications of the HYDRUS computer software packages. *Vadose Zone Journal*, 15, 1–25. <https://doi.org/10.2136/vzj2016.04.0033>
- Šimůnek, J., Jarvis, N. J., van Genuchten, M. Th., & Gardenas, A. (2003). Review and comparison of models for describing nonequilibrium and preferential flow and transport in the vadose zone. *Journal of Hydrology*, 272, 14–35. [https://doi.org/10.1016/S0022-1694\(02\)00252-4](https://doi.org/10.1016/S0022-1694(02)00252-4)
- Šimůnek, J., van Genuchten, M. Th., & Sejna, M. (2006). *The HYDRUS software package for simulating two- and three-dimensional movement of water, heat, and multiple solutes in variably-saturated media: technical manual* (version 1.0). PC-Progress.
- Todd, M. S., Jeff, P. R., & George, M. H. (2000). Shallow subsurface storm flow in a forested headwater catchment: Observations and modeling using a modified TOPMODEL. *Water Resources Research*, 36(9), 2575–2586.
- Tromp-van Meerveld, H. J., Peters, N. E., & McDonnell, J. J. (2007). Effect of bedrock permeability on subsurface stormflow and the water balance of a trenched hillslope at the Panola Mountain Research Watershed, Georgia, USA. *Hydrological Processes*, 21, 750–769. <https://doi.org/10.1002/hyp.6265>
- Tromp-van Meerveld, I., & Weiler, M. (2008). Hillslope dynamics modeled with increasing complexity. *Journal of Hydrology*, 361, 24–40. <https://doi.org/10.1029/2007WR006299>
- Twarakavi, N. K. C., Šimůnek, J., & Seo, H. S. (2008). Evaluating interactions between groundwater and vadose zone using HYDRUS-based flow package for MODFLOW. *Vadose Zone Journal*, 7, 757–768. <https://doi.org/10.2136/vzj2007.0082>
- van Genuchten, M. Th. (1980). A closed-form equation for predicting the hydraulic conductivity of unsaturated soils. *Soil Science Society of America Journal*, 44, 892–898. <https://doi.org/10.2136/sssaj1980.03615995004400050002x>
- van Genuchten, M. Th., Leij, F. J., & Yates, S. R. (1991). *The RETC code for quantifying the hydraulic functions of unsaturated soils* (EPA 600/2-91/065). U.S. Salinity Laboratory, USDA-ARS.
- Vereecken, H., Amelung, W., Bauke, S. L., Bogaen, H., Brueggemann, N., Montzka, C., Vanderborght, J., Bechtold, M., Bloesch, G., Carminati, A., Javaux, M., Konings, A. G., Kusche, J., Neuweiler, I., Or, D., Steele-Dunne, S., Verhoef, A., Young, M., & Zhang, Y. (2022). Soil hydrology in the Earth system. *Nature Reviews Earth & Environment*, 3, 573–587. <https://doi.org/10.1038/s43017-022-00324-6>
- Vereecken, H., Huisman, J. A., Hendricks Franssen, H. J., Bruggemann, N., Bogaen, H. R., Kollet, S., Javaux, M., van der Kruk, J., & Vanderborght, J. (2015). Soil hydrology: Recent methodological advances, challenges, and perspectives. *Water Resources Research*, 51, 2616–2633. <https://doi.org/10.1002/2014WR016852>
- Vogel, H.-J., & Roth, K. (2003). Moving through scales of flow and transport in soil. *Journal of Hydrology*, 272, 95–106. [https://doi.org/10.1016/S0022-1694\(02\)00257-3](https://doi.org/10.1016/S0022-1694(02)00257-3)
- Weiler, M., & McDonnell, J. J. (2007). Conceptualizing lateral preferential flow and flow networks and simulating the effects on gauged and ungauged hillslopes. *Water Resources Research*, 43, W03403. <https://doi.org/10.1029/2006WR004867>
- Yi, J., Yang, Y., Liu, M., Hu, W., Lou, S., Zhang, H., & Zhang, D. (2019). Characterising macropores and preferential flow of mountainous forest soils with contrasting human disturbances. *Soil Research*, 57(6), 601–614. <https://doi.org/10.1071/SR18198>
- Zepp, H., Tang, J. L., & Zhang, B. (2005). A methodological framework for a multiscale study on hydrological processes and soil erosion in subtropical SE China. *Pedosphere*, 15, 695–706.
- Zhao, Y., Peth, S., Horn, R., Krümmelbein, J., Ketzler, B., Gao, Y. Z., Doerner, J., Bernhofer, C., & Peng, X. H. (2010). Modelling grazing effects on coupled water and heat fluxes in Inner Mongolia grassland. *Soil and Tillage Research*, 109, 75–86. <https://doi.org/10.1016/j.still.2010.04.005>
- Zhao, Y., Rahmati, M., Vereecken, H., & Or, D. (2024). Comment on “Are soils overrated in hydrology?” by Gao et al. (2023). *EGU-sphere*, <https://egusphere.copernicus.org/preprints/2024/egusphere-2024-629/>
- Zhao, Y., Tang, J., Graham, C., Zhu, Q., Takagi, K., & Lin, H. (2012). Hydrogeology in the ridge and valley: Soil moisture patterns and preferential flow dynamics in two contrasting landscapes. In H. Lin (Ed.), *Hydrogeology: Synergistic integration of soil science and hydrology* (pp. 381–411). Academic Press, Elsevier.

Zhao, Y., Wang, H., Song, B., Xue, P., Zhang, W., Peth, S., Hill, R. L., & Horn, R. (2023). Characterizing uncertainty in process-based hydraulic modeling, exemplified in a semiarid Inner Mongolia steppe. *Geoderma*, 440, 116713. <https://doi.org/10.1016/j.geoderma.2023.116713>

SUPPORTING INFORMATION

Additional supporting information can be found online in the Supporting Information section at the end of this article.

How to cite this article: Zhao, Y., Yi, J., Yao, R., Li, F., Hill, R. L., & Gerke, H. H. (2024). Dimensionality and scales of preferential flow in soils of Shale Hills hillslope simulated using HYDRUS. *Vadose Zone Journal*, e20367. <https://doi.org/10.1002/vzj2.20367>